Central exclusive production of the scalar χ_c meson at the Fermilab Tevatron, BNL RHIC, and CERN LHC energies

R. S. Pasechnik,* A. Szczurek,+ and O. V. Teryaev‡

Bogoliubov Laboratory of Theoretical Physics, JINR, Dubna 141980, Russia,
Institute of Nuclear Physics PAN, PL-31-342 Cracow, Poland,
University of Rzeszów, PL-35-959 Rzeszów, Poland

(Received 13 September 2007; published 9 July 2008)

We calculate several differential distributions for exclusive double-diffractive $\chi_c(0^{++})$ production in the proton-antiproton collisions at the Tevatron and in proton-proton collisions at RHIC and LHC. We use unintegrated gluon distributions (UGDFs) within the k_t-factorization approach. The $g^*g^* \to \chi_c(0^{++})$ transition vertex is calculated as a function of gluon virtualities via the standard perturbative nonrelativistic QCD technique. The off shell effects are discussed and quantified. They lead to a reduction of the cross section by a factor of 2–5, depending on the position in the phase space and UGDFs. Different models of UGDFs are used and the results are shown and discussed. The cross section for the diffractive component depends strongly on UGDFs. Transverse momentum distribution of $\chi_c(0)$ shows a well localized minimum. We calculate also the differential distributions for the $\gamma^*\gamma^* \to \chi_c(0^{++})$ fusion mechanism. The integrated cross section for photon-photon fusion is much smaller than that of diffractive origin. The two components have very different dependence on the momentum transfers t_1, t_2 in the nucleon lines as well as azimuthal-angle correlations between both outgoing nucleons.

DOI: 10.1103/PhysRevD.78.014007 PACS numbers: 13.87.Ce, 13.60.Le, 13.85.Lg

I. INTRODUCTION

The discovery of Higgs is the main motivation for the construction and putting into operation of the Large Hadron Collider (LHC) at CERN. The analysis of an inclusive cross section will be the ''main road'' of future investigations. Different decay channels will be studied. The analysis in each of these channels is rather complicated as huge irreducible backgrounds are unavoidably present.

The diffractive exclusive production of the Higgs boson seems to be much cleaner in this respect. Many estimates of the corresponding cross section have been presented in the literature. The so-called Durham model [1] suggested by V. A. Khoze, A. D. Martin, and M. G. Ryskin (KMR) and developed in collaboration with A. B. Kaidalov and W. J. Stirling, is the state-of-art in this field. The cross section for the diffractive production is much smaller than the cross section for the inclusive case, but the ratio of the signal to the more conventional background seems promising. Recently a detailed analysis of diffractive production of the minimal supersymmetric standard model Higgs [2] appeared. We do not need to mention that any check against experimental data of the theoretical methods used is not possible at present, at least for the Higgs production. The way out is to study the diffractive production of heavy quarkonia where almost the same theoretical methods (although in slightly different kinematical regions) can be used. The basic diagram for the amplitude of the process is shown in Fig. 1. In recent years, the production of heavy quarkonia received a lot of attention from both theory and experiment. For a review we refer to Refs. [3–7].

QCD dynamics at small quark and gluon momentum fractions (or large total energy), relevant for HERA, Tevatron, RHIC, and LHC, are still poorly understood. It was shown in [8,9] that the combination of the $k_\perp$ factorization approach [10–13] and the next-to-leading-logarithmic-approximation BFKL vertex [14] gives quite

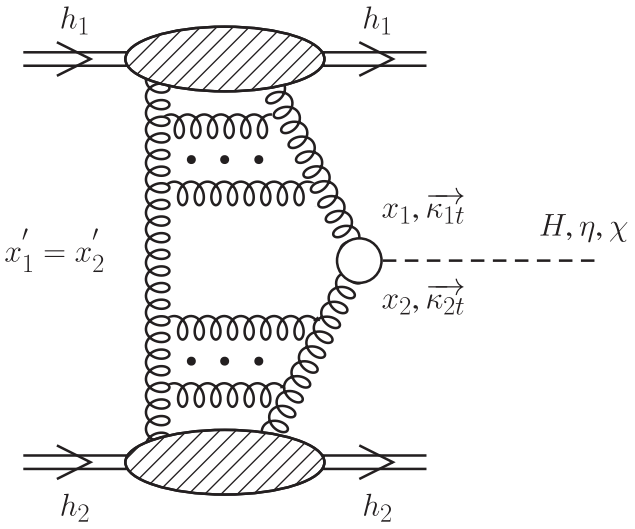

FIG. 1. The sketch of bare QCD mechanism and main kinematical variables.

*rpasech@theor.jinr.ru
+antoni.szczurek@ifj.edu.pl
‡teryaev@theor.jinr.ru

good agreement with data on inclusive $Q\bar{Q}$ production. One can therefore hope that these concepts provide a valuable foundation also for the exclusive processes.

KMR proposed to calculate the diffractive double elastic[1] production of the Higgs boson in terms of unintegrated gluon distributions [1]. Related uncertainties were discussed in Refs. [1,15,16]. It would be interesting to apply this approach to other reactions [17] which are measured or can be measured in the near future.

At present only the diffractive production of dijets was studied experimentally [18]. The exclusive contribution calculated in the spirit of the KMR approach [19] seems to describe the distributions in the region of large dijet mass fraction $R_{jj} = M_{jj}/M_X$, where M_{jj} is the dijet mass and M_X is the full missing mass. At present, however, the inelastic and elastic contributions cannot be separated experimentally, therefore no clear conclusions can be drawn. The exclusive contribution may be deduced only by the missing strength when only inclusive (inelastic) contribution is included in the calculation [19]. The inclusive contribution is model dependent, however. In particular, the large dijet mass fraction spectrum is sensitive to gluon distribution in the Pomeron at large β, which is rather difficult to constrain experimentally. Clearly a more detailed analysis is needed.

Here we wish to discuss the possibility of heavy quarkonia production. In Refs. [20,21], the integrated cross section for the exclusive double-diffractive $\chi_c(0^{++})$ production was estimated using identical formulas as for the scalar Higgs production with $\Gamma_{H\to gg}$ replaced by $\Gamma_{\chi_c(0^{++})\to gg}$. Of course, in general case such a procedure can be strictly valid only for fictitious structureless objects, when the internal wave function and gluon virtualities are neglected. From the spectroscopy point of view the $\chi_c(0^{++})$ meson is a quark-antiquark P-wave state, and it might be interesting to study an exclusive production of P waves applying the perturbative nonrelativistic QCD (pNRQCD) methods. Such a calculation may be especially important when we go to larger gluon virtualities.

In parallel to the exclusive channel studies there was a lot of theoretical activity for inclusive charmonium and bottomonium production (see, for example, [22–24]). There the nonrelativistic pQCD methods are usually applied. In these approaches the nonrelativistic quark-antiquark wave function is taken explicitly into the calculation. The vertex function $g^*g^*q\bar{q}$ corresponds to the so-called quasi-multi-Regge kinematics (QMRK), i.e., when q and $\bar{q}$ have similar rapidities and form a cluster. It is based on the formalism developed by Lipatov and Fadin [14] for the diffractive $q\bar{q}$ pair production.

We would like to stress here that the use of the next-to-leading order (NLO) effective BFKL vertex [14] guarantees the gauge invariance of the production amplitude (cross section) of any hadronic system from the fusion of off shell Regge-ized gluons, both in inclusive and exclusive processes. Moreover, in the case of the production of the color singlet quark-antiquark pair, the additional three-gluon contribution to effective vertex is projected out and the result is completely described by standard QCD Feynman rules [9].

In the present work, we shall use the pNRQCD methods for the exclusive double-diffractive $\chi_c(0^{++})$ production. The quarkonium mass provides some hard scale in the considered process, as initially suggested by KMR [21]. The main ingredients of our calculations are the unintegrated gluon distributions (UGDFs) and the effective next-to-leading-logarithmic-approximation BFKL production vertex in QMRK (with Regge-ized gluon couplings to quarks). We would like to compare our results obtained using this vertex with the KMR results. The projection of the heavy quark-antiquark pair onto the corresponding charmonium state is described in the standard way within the nonrelativistic-quarkonium model [25–27]. Finally, we shall refer to the original KMR result [21] where the wave function is not included explicitly. For completeness, we shall include also the photon-photon fusion mechanism of the exclusive $\chi_c(0^{++})$ production shown in Fig. 2. In addition to the diffractive QCD approach, we also discuss the phenomenological Pomeron-Pomeron fusion approach.

When compared to the Higgs production, where due to the Sudakov form factors small virtualities are effectively cut off, here the sizeable contribution to the amplitude may come just from this region. This means that the process is nonperturbative per definition. Therefore in the present analysis, we shall use several UGDFs relevant for small

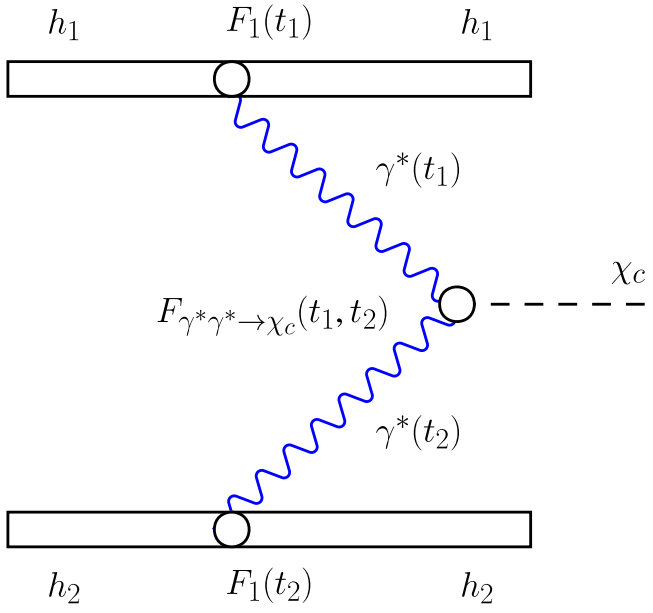

FIG. 2 (color online). The sketch of photon-photon fusion mechanism. Form factors appearing in different vertices are shown explicitly.

[1]Both protons survive the collision.

gluon virtualities (transverse momenta). We shall also discuss the related uncertainties in the KMR approach.

In the present paper, we wish to calculate differential distributions for the exclusive $\chi_c(0^+)$ production with different UGDFs taken from the literature. We shall calculate matrix elements for the off shell gluons. We shall discuss also the uncertainties related to the approximations made, the choice of the scale, etc. The contribution of the $\gamma^*\gamma^*$ fusion to the differential cross sections will be calculated as well.

II. DIFFRACTIVE QCD MECHANISM

In the pNRQCD approach the diffractive exclusive reaction is viewed as shown in Fig. 3. The corresponding calculation can be summarized as follows. First, the $q\bar{q}$-continuum amplitude is calculated. Then the $gg \to q\bar{q}$ amplitude is reduced to the $gg \to \chi_c$ amplitude with standard projection techniques developed in [25,28].

A. Matrix element for exclusive double-diffractive $\chi_c(0^{++})$ production

Let us consider first the $q\bar{q}$ production. The general kinematics for the process $pp \to pp(q\bar{q})$ on the quark level is shown in Fig. 4.

We adopt here the following standard definition of the light-cone coordinates

$$k^+ \equiv n_\alpha^+ k^\alpha = k^0 + k^3, \qquad k^- \equiv n_\alpha^- k^\alpha = k^0 - k^3,$$
$$k_t = (0, k^1, k^2, 0) = (0, \mathbf{k}, 0),$$

where $n^\pm$ are the light-cone basis vectors. In the center-of-mass (c.m.s.) frame

$$n^+ = \frac{p_2 + q_0}{E_{\rm cms}}, \qquad n^- = \frac{p_1 - q_0}{E_{\rm cms}}, \tag{2.1}$$

and the momenta of the scattering hadrons are given by

$$p_1^+ = p_2^- = \sqrt{s}, \qquad p_1^- = p_2^+ = p_{1,t} = p_{2,t} = 0,$$

with the Mandelstam variable $s = 4E_{\rm cms}^2$.

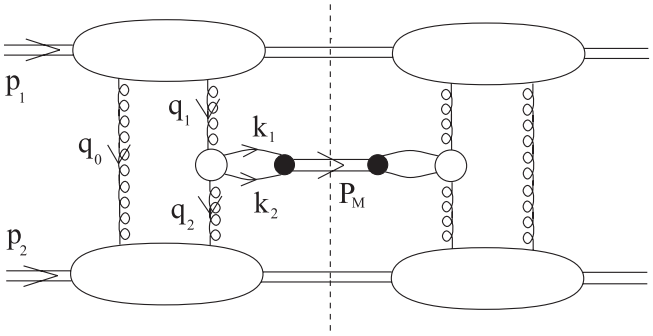

FIG. 3. Basic diagram of double-diffractive charmonium production $pp \to pp\chi_c$.

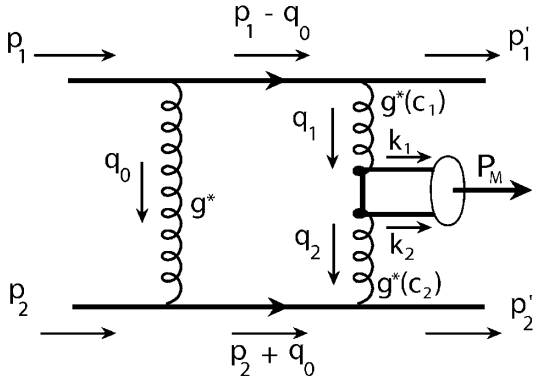

FIG. 4. General kinematics of exclusive double-diffractive production.

The decomposition of gluon momenta into longitudinal and transverse parts is

$$q_1 = x_1(p_1 - q_0) + q_{1,t},$$
$$q_2 = -x_2(p_2 + q_0) + q_{2,t} \qquad 0 < x_{1,2} < 1, \tag{2.2}$$
$$q_0 = x_1' p_1 + x_2' p_2 + q_{0,t} \approx q_{0,t}, \qquad x_1', x_2' \approx 0.$$

Making use of conservation laws

$$q_1 + p_1' = p_1 - q_0, \qquad q_2 + p_2 + q_0 = p_2', \qquad q_1 - q_2 = P_M, \tag{2.3}$$

we write

$$s x_1 x_2 = M^2 + |\mathbf{P}_{M,t}|^2 \equiv M_\perp^2. \tag{2.4}$$

According to the KMR approach [1], we write the amplitude of the exclusive double-diffractive color singlet production $pp \to pp\chi_{cJ}$ as

$$\mathcal{M}^{g^*g^*} = \frac{s}{2} \cdot \pi^2 \frac{1}{2} \frac{\delta_{c_1c_2}}{N_c^2 - 1} \Im \int d^2 q_{0,t} V_J^{c_1c_2} \times \frac{f_{g,1}^{\rm off}(x_1, x_1', q_{0,t}^2, q_{1,t}^2, t_1) f_{g,2}^{\rm off}(x_2, x_2', q_{0,t}^2, q_{2,t}^2, t_2)}{q_{0,t}^2 q_{1,t}^2 q_{2,t}^2}. \tag{2.5}$$

The normalization convention of this amplitude differs from that of the KMR paper [1,21] by the factor $s/2$ and coincides with the normalization in our previous work on exclusive η' production [29]. The amplitude is averaged over the color indices and over the two transverse polarizations of the incoming gluons [1]. The bare amplitude above is subjected to absorption corrections which depend on collision energy. We shall discuss this issue shortly when presenting our results.

The vertex factor $V_J^{c_1c_2} = V_J^{c_1c_2}(q_{1,t}^2, q_{2,t}^2, P_{Mt}^2)$ in expression (2.5) describes the coupling of two virtual gluons to χ_{cJ} meson that can be written symbolically as

$$V_J^{c_1c_2} = \mathcal{P}(q\bar{q} \to \chi_{cJ}) \bullet \Psi_{ik}^{c_1c_2}(k_1, k_2), \tag{2.6}$$

where $\mathcal{P}(q\bar{q} \to \chi_{cJ})$ is the operator that projects the $q\bar{q}$ pair onto the charmonium bound state (see below), $\Psi^{c_1c_2}(k_1, k_2)$ is the production amplitude of a pair of massive quark q and antiquark $\bar{q}$ with momenta k_1, k_2, respectively.

Within the QMRK approach [14], we have

$$\Psi(c_1, c_2; i, k; k_1, k_2) = -g^2(t^{c_1}_{ij} t^{c_2}_{jk} b(k_1, k_2) - t^{c_2}_{kj} t^{c_1}_{ji} \bar{b}(k_2, k_1)), \qquad \alpha_s = \frac{g^2}{4\pi}, \tag{2.7}$$

where t^c are the color group generators in the fundamental representation, b, $\bar{b}$ are the effective vertices (2.8) arising from the Feynman rules of QMRK illustrated in Fig. 5,

$$b(k_1, k_2) = \gamma^- \frac{\hat{q}_1 - \hat{k}_1 - m}{(q_1 - k_1)^2 - m^2}\gamma^+ - \frac{\gamma_\beta \Gamma^{+-\beta}(q_2, q_1)}{(k_1 + k_2)^2},$$
$$\bar{b}(k_1, k_2) = \gamma^+ \frac{\hat{q}_1 - \hat{k}_1 + m}{(q_1 - k_1)^2 - m^2}\gamma^- - \frac{\gamma_\beta \Gamma^{+-\beta}(q_2, q_1)}{(k_1 + k_2)^2}. \tag{2.8}$$

Taking into account definitions (2.1) and (2.3) and using the gauge invariance property

$$q_1^\nu V^{c_1c_2}_{J,\mu\nu} = q_2^\mu V^{c_1c_2}_{J,\mu\nu} = 0,$$

we get the following projection

$$V_J^{c_1c_2} = n_\mu^+ n_\nu^- V^{c_1c_2}_{J,\mu\nu}(q_1, q_2) = -\frac{4}{s}\frac{q^\nu_{1,t}}{x_1}\frac{q^\mu_{2,t}}{x_2} V^{c_1c_2}_{J,\mu\nu}(q_1, q_2). \tag{2.9}$$

The normalization of polarization vectors coincides with that of Ref. [30]. Since we adopt here the definition of polarization vectors proportional to gluon transverse momenta $q_{1/2,t}$, we must take into account the longitudinal momenta in the numerators of vertices (2.8). While projecting on the color singlet the ggg vertices $\Gamma^{+-\beta}$ in (2.8) cancel each other and disappear from the resulting matrix element, so only the first diagram in the decomposition in Fig. 5 contributes.

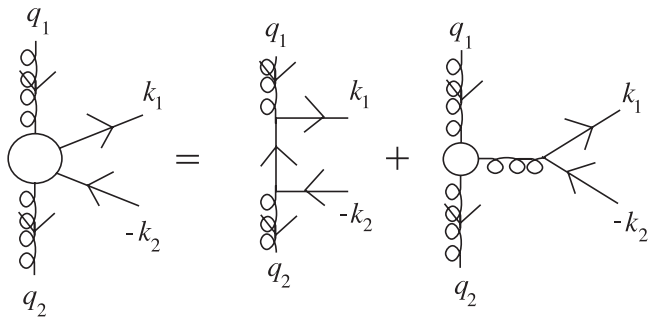

FIG. 5. Effective vertex in QMRK approach.

The projection of the hard amplitude onto the singlet charmonium bound state $V^{c_1c_2}_{\mu\nu}$ is given by a four-dimensional integral over the relative momentum of quark and antiquark $q = (k_1 - k_2)/2$ [8,24]

$$\begin{aligned} V^{c_1c_2}_{J,\mu\nu}(q_1, q_2) &= \mathcal{P}(q\bar{q} \to \chi_{cJ}) \bullet \Psi^{c_1c_2}_{ik,\mu\nu}(k_1, k_2) \\ &= 2\pi \cdot \sum_{i,k}\sum_{L_z,S_z}\frac{1}{\sqrt{m}}\int\frac{d^4q}{(2\pi)^4}\delta\left(q^0 - \frac{\mathbf{q}^2}{M}\right) \\ &\quad \times \Phi_{L=1,L_z}(\mathbf{q}) \cdot \langle L = 1, L_z; S = 1, S_z | J, J_z\rangle \\ &\quad \times \langle 3i, \bar{3}k | 1\rangle \mathrm{Tr}\{\Psi^{c_1c_2}_{ik,\mu\nu}\mathcal{P}_{S=1,S_z}\}, \\ \Psi^{c_1c_2}_{ik,\mu\nu} &= -g^2\left[t^{c_1}_{ij}t^{c_2}_{jk} \cdot \left\{\gamma_\nu \frac{\hat{q}_1 - \hat{k}_1 - m}{(q_1 - k_1)^2 - m^2}\gamma_\mu\right\}\right. \\ &\quad \left. - t^{c_2}_{kj}t^{c_1}_{ji} \cdot \left\{\gamma_\mu \frac{\hat{q}_1 - \hat{k}_2 + m}{(q_1 - k_2)^2 - m^2}\gamma_\nu\right\}\right], \end{aligned} \tag{2.10}$$

where the function $\Phi_{L=1,L_z}(\mathbf{q})$ is the momentum space wave function of the charmonium, and for a small relative momentum q the projection operator $\mathcal{P}_{S=1,S_z}$ has the form

$$\mathcal{P}_{S=1,S_z} = \frac{1}{2m}(\hat{k}_2 - m)\frac{\hat{\epsilon}(S_z)}{\sqrt{2}}(\hat{k}_1 + m). \tag{2.11}$$

Straightforward calculations finally lead to the following vertex function

$$\begin{aligned} V^{c_1c_2}_{J=0}(q_1, q_2) &= 8ig^2\frac{\delta^{c_1c_2}}{M}\frac{\mathcal{R}'(0)}{\sqrt{\pi M N_c}} \\ &\quad \times \frac{3M^2(q_{1,t}q_{2,t}) + 2q^2_{1,t}q^2_{2,t} - (q_{1,t}q_{2,t})(q^2_{1,t} + q^2_{2,t})}{(M^2 - q^2_{1,t} - q^2_{2,t})^2}. \end{aligned}$$

We have also calculated the subprocess matrix element squared $\mathcal{B}(q_1, q_2) = V_{\mu\nu}V^{\mu\nu}$ that is usually used in inclusive production calculations. The form of $\mathcal{B}(q_1, q_2)$ is identical to the form of the matrix element squared obtained very recently by Likhoded and Luchinsky in Ref. [22].

The objects $f^{\mathrm{off}}_{g,1}(x_1, x_1', q^2_{0,t}, q^2_{1,t}, t_1)$ and $f^{\mathrm{off}}_{g,2}(x_2, x_2', q^2_{0,t}, q^2_{2,t}, t_2)$ appearing in formula (2.5) are skewed (or off-diagonal) unintegrated gluon distributions. They are nondiagonal both in the x and q_t^2 space. The usual off-diagonal gluon distributions are nondiagonal only in x. In the limit $x_{1,2} \to x'_{1,2}$, $q^2_{0,t} \to q^2_{1/2,t}$, and $t_{1,2} \to 0$ they become the usual UGDFs. Our choice of the different UGDFs will be discussed in more detail in a separate section.

The choice of effective strong coupling constants $g(\mu_1^2)g(\mu_2^2)$ in the $g^*g^*\chi_c(0)$ vertex requires some discussion. In most of the calculation performed in the present paper we take $\mu_1^2 = M_\chi^2$ and $\mu_2^2 = M_\chi^2$. This means that $\alpha_s \sim 0.3$. If, however, $\mu_1^2 = q_{1t}^2$ and $\mu_2^2 = q_{2t}^2$ were taken, which is often done in the practical applications of the

k_t-factorization approach to the inclusive case, one would worry about the behavior of α_s in the infrared region.

This latter choice is the natural one in the framework of "naive non-Abelization," when the whole effect of coupling renormalization is attributed to the bubble's insertion to gluon line. The choice $\mu_2^2 = M_\chi^2$ corresponds to taking the separate scales in the hard and soft parts of the amplitude, the coupling dependent on the soft scale being absorbed to the definition of UGDF. The comparison of these two choices in the case of inclusive production showed [8] their numerical closeness. At the same time, the contribution of the low transverse momenta region in our case requires the more detailed analysis.

In the perturbative regime, the running coupling has the general form

$$\alpha_s(k^2) = 1./b_0 a(k^2/\Lambda^2), \tag{2.12}$$

where for N_f active flavors

$$b_0 = \frac{33 - 2N_f}{12\pi} \tag{2.13}$$

and to a one-loop order

$$a(x) \sim \frac{1}{\ln x}. \tag{2.14}$$

One encounters a problem when continuing expression (2.12) to low k^2—the so-called Landau pole at $k^2 = \Lambda^2$.

Several models have been proposed how to continue the perturbative dependence to the nonperturbative region. Some illustrative models can be found in Refs. [31–37] (for a review, see, [38]). A particularly simple, with many attractive properties, is a model by Shirkov and Solovtsov [34] exploring the fundamental properties of analyticity and causality. In this model, the resulting k^2 dependence is monotonic and $\alpha_s(0)$ takes a finite value. In some models (parametrizations) α_s can have a maximum at $0 < k^2 < 1$ GeV^2 [32,36]. In some class of models $\alpha_s(0) = 0$ [32]. In the result section, we shall show for illustration $d\sigma/dy$ with a few distinct models of the infrared behavior of α_s from the literature.

B. Khoze-Martin-Ryskin approach

In the original KMR approach [1], the amplitude is written as

$$\mathcal{M} = N \int \frac{d^2 q_{0,t} P[\chi_c(0^+)]}{q_{0,t}^2 q_{1,t}^2 q_{2,t}^2} f_g^{\mathrm{KMR}}(x_1, x_1', Q_{1,t'}^2, \mu^2; t_1) \times f_g^{\mathrm{KMR}}(x_2, x_2', Q_{2,t'}^2, \mu^2; t_2), \tag{2.15}$$

where only one transverse momentum is somewhat arbitrarily taken into account as

$$Q_{1,t}^2 = \min\{q_{0,t}^2, q_{1,t}^2\}, \qquad Q_{2,t}^2 = \min\{q_{0,t}^2, q_{2,t}^2\}, \tag{2.16}$$

and the normalization factor N can be written in terms of the $\chi_c(0^+) \to gg$ decay width (see below).

In the KMR approach the large meson mass approximation $M \gg |\mathbf{q}_{1,t}|, |\mathbf{q}_{2,t}|$ is adopted, so the gluon virtualities are neglected in the vertex factor

$$P[\chi_c(0^+)] \simeq (q_{1,t} q_{2,t}) = (q_{0,t} + p_{1,t}')(q_{0,t} - p_{2,t}'). \tag{2.17}$$

In the present analysis we go beyond this approximation, by taking into account off-shellness of the participating gluons.

The KMR UGDFs are written in the factorized form

$$f_g^{\mathrm{KMR}}(x, x', Q_t^2, \mu^2; t) = f_g^{\mathrm{KMR}}(x, x', Q_t^2, \mu^2) \exp(b_0 t) \tag{2.18}$$

with $b_0 = 2$ GeV^{-2} [1]. We use different parametrization of the t-dependent isoscalar form factors [see Eqs. (2.28) and (2.29) below].

Please note that the KMR and our skewed UGDFs have a different number of arguments. In the KMR approach, there is only one effective gluon transverse momentum [see Eq. (2.16)] compared to two independent transverse momenta in our case [see Eq. (2.28)].

The KMR skewed distributions are given in terms of the conventional integrated densities g and the so-called Sudakov form factor T as follows:

$$f_g^{\mathrm{KMR}}(x, x', Q_t^2, \mu^2) = R_g \frac{\partial}{\partial \ln Q_t^2} [\sqrt{T(Q_t^2, \mu^2)} x g(x, Q_t^2)]. \tag{2.19}$$

The square root here was taken using arguments that only the survival probability for hard gluons is relevant. It is not so obvious if this approximation is reliable for $c\bar{c}$ quarkonium production. In addition this has to be contrasted with the choice of gluon momentum of the KMR UGDF in (2.16) as the minimal one (not harder) of the two gluons. Please note also that the skewed KMR UGDF does not explicitly depend on x' (assuming $x' \ll x \ll 1$). In our prescription of skewed UGDFs (see below) we take into account such dependence. The factor R_g approximately accounts for the single $\log Q^2$ skewed effect [1]. Usually this factor is estimated to be 1.3–1.5. In our evaluations here, we take it to be equal to 1 to avoid further uncertainties.

In contrast to the Higgs case, in the case of light quarkonium production, the dominant contribution to the integral (2.15) comes from rather small values of gluon transverse momenta. Therefore, it becomes essential what one does phenomenologically in the nonperturbative region $Q_t^2 < Q_0^2$, where the Q_0^2 is a minimal nonperturbative scale for standard integrated distributions. Of course, for scales smaller than Q_0^2, the standard collinear gluon distributions do not formally exist and an extra extension is unavoidable. This issue was not discussed in detail in the literature. We shall illustrate this point in Sec. V.

The Sudakov factor is the result of the resummation of the virtual contributions in the Dokshitzer-Gribov-Lipatov-Altarelli-Parisi (DGLAP) evolution and reads

$$T(Q_t^2, \mu^2) = \exp\Big(-\int_{Q_t^2}^{\mu^2} \frac{\alpha_s(k_t^2)}{2\pi}\frac{dk_t^2}{k_t^2} \times \int_0^{1-\Delta}[zP_{gg}(z) + \sum_q P_{qg}(z)]dz\Big), \quad (2.20)$$

with $\Delta = k_t/(\mu + k_t)$. In their (KMR) estimates the hard scale is usually taken $\mu = M_\chi/2$. Of course, the choice of the scale is somewhat arbitrary, and consequences of this choice were not discussed in the literature.

In Fig. 6, we show the KMR unintegrated gluon distribution (2.19) as a function of Q_t^2 for different values of x specified in the figure for two different choices of the scale. The DGLAP distribution for $Q_t^2 < Q_0^2$ is not well-defined and we arbitrarily put it to zero as in Ref. [21]. In principle, one could try several other extrapolations into the nonperturbative region to see its influence on the resulting differential cross sections.

We have used the Glück-Reya-Vogt collinear distributions to generate the KMR off-diagonal UGDFs [39]. The collinear distributions (such as CTEQ, MRST) are defined above a relatively large scale, as compared to the Glück-Reya-Vogt distributions, and therefore are less useful in the application discussed here.

The bare amplitude for the diffractive process can be written formally as

$$\mathcal{M}(y, t_1, t_2, \phi) = \int dq_{0,t} I(q_{0,t}; y, t_1, t_2, \phi). \quad (2.21)$$

Let us concentrate on the dependence of the integrand on q_t. Such an integrand of the amplitude is a good measure of how much the process is of perturbative/nonperturbative nature.

In Fig. 7, we show an example of the integrand of the amplitude obtained with the KMR UGDFs and different prescriptions on how to choose the effective transverse momentum (to be discussed in more detail in Sec. V).

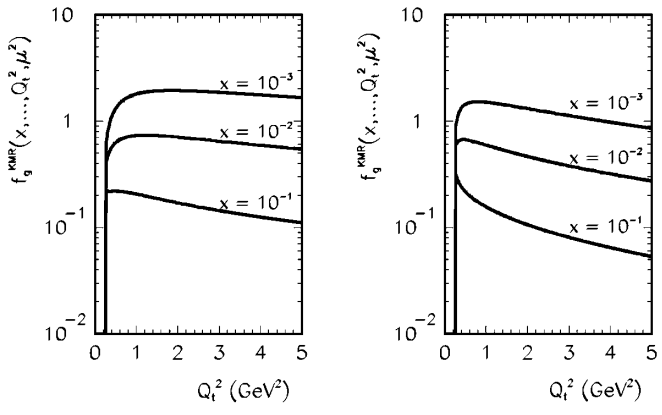

FIG. 6. KMR unintegrated gluon distribution as a function of effective transverse momentum Q_t^2 for different values of x and $\mu^2 = M_\chi^2$ (left panel) and $\mu^2 = (M_\chi/2)^2$ (right panel).

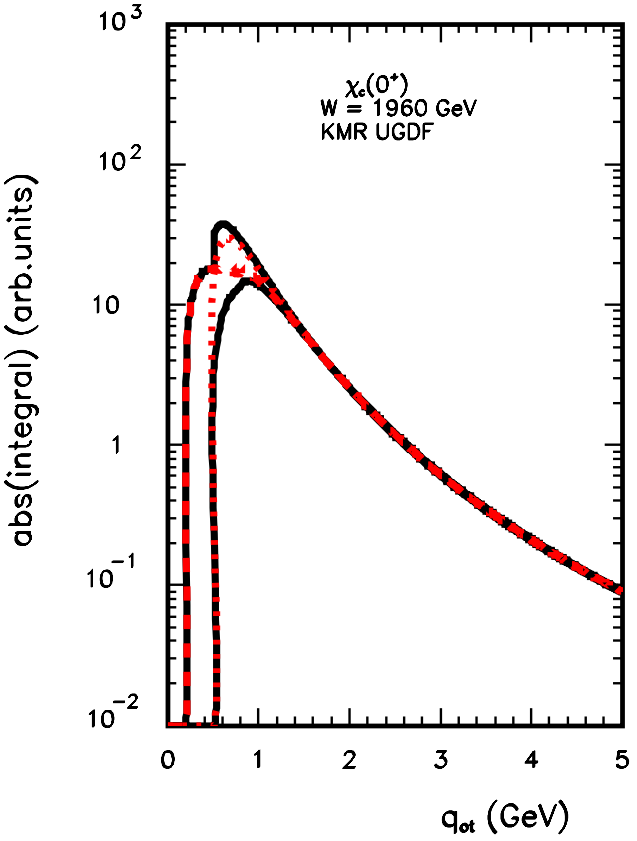

FIG. 7 (color online). A representative example of the integrand $|I(q_{0t}; t_1 = -0.1\ \mathrm{GeV}^2,\ t_2 = -0.1\ \mathrm{GeV}^2,\ \phi = \pi)|$ in Eq. (2.21) as a function of exchanged transverse momentum $q_{0,t}$ for the KMR approach and for different prescriptions on effective transverse momentum: "minimum prescription" (lower solid line), "maximum prescription" (upper solid line), "production line prescription" (dashed line) and "no-production line prescription" (dotted line).

The two solid lines correspond to the "minimum prescription" (lower solid curve) and the "maximum prescription" (upper solid line). The dashed (red line) curve represents the prescription $Q_{1,t}^2 = q_{1,t}^2$ and $Q_{2,t}^2 = q_{2,t}^2$ (production line prescription), while the dotted line is for the prescription $Q_{1,t}^2 = Q_{2,t}^2 = q_{0,t}^2$ (no-production line prescription). At $q_{0,t} > 1$ GeV all prescriptions coincide. The difference is in the low $q_{0,t}$ region. In the "minimum prescription" and in the "no-production line prescription" the integrand vanishes below Q_0^2, i.e., in the region where the KMR off-diagonal UGDFs are not well-defined. At low $q_{0,t}$, the effective transverse momenta $Q_{1,t} = q_{1,t}$ and $Q_{2,t} = q_{2,t}$ therefore the "maximum prescription" and the "production line prescription" give the strength below $q_{0,t}^2 < Q_0^2$, where Q_0^2 is the minimal scale for corresponding collinear distributions. This leads to a huge enhancement of the amplitude and of the corresponding cross section which will be discussed in the following. Clearly, this enhancement has a nonperturbative origin.

C. QMRK vertex versus Khoze-Martin-Ryskin vertex

We wish to compare the QMRK vertex function (2.12) with the KMR vertex function [21]. In the KMR limit of large meson mass $M \gg |\mathbf{q}_{1,t}|, |\mathbf{q}_{2,t}|$ and $sx_1x_2 \simeq M^2$ the vertex reads

$$V^{c_1c_2}_{J=0}[M \gg q_{1,t}, q_{2,t}] \simeq 8ig^2\delta^{c_1c_2}\frac{\mathcal{R}'(0)}{M^3}\frac{1}{\sqrt{\pi M N_c}}\{3(q_{1,t}q_{2,t})\} = i\delta^{c_1c_2}\cdot 8g^2\sqrt{\frac{3}{\pi M}}\frac{\mathcal{R}'(0)}{M^3}\cdot(q_{1,t}q_{2,t}). \quad (2.22)$$

Following the KMR notations [21] we now write the total NRQCD QMRK amplitude (2.5) (averaged over color and polarization states of incoming gluons) in the limit $M \gg q_{1,t}, q_{2,t}$ as

$$\mathcal{M} = A\pi^2\frac{s}{2}\int d^2q_{0,t}P[\chi_c(0^+)] \times \frac{f^{\rm off}_{g,1}(x_1, x_1', q^2_{0,t}, q^2_{1,t}, t_1)f^{\rm off}_{g,2}(x_2, x_2', q^2_{0,t}, q^2_{2,t}, t_2)}{q^2_{0,t}q^2_{1,t}q^2_{2,t}}, \quad (2.23)$$

where the normalization is

$$A = 4g^2\sqrt{\frac{3}{\pi M}}\frac{\mathcal{R}'(0)}{M^3}, \quad (2.24)$$

and the vertex factor is defined in (2.17).

The normalization constant A can be obtained in terms of partial decay width $\Gamma(\chi_{c0} \to gg)$ as [see, formula (19) in the KMR paper [21]]

$$A^2 = K\frac{64\pi\Gamma(\chi_{c0} \to gg)}{(N_c^2-1)M^3}, \qquad \text{NLO} \to K = 1.5. \quad (2.25)$$

Using the expression for $\Gamma(\chi_{c0} \to gg)$, obtained in the framework of pNRQCD [40,41]

$$\Gamma(\chi_{c0} \to gg) = 32N_c\alpha_s^2\frac{|\mathcal{R}'(0)|^2}{M^4}, \qquad N_c = 3 \quad (2.26)$$

we get the normalization constant (with $K = 1$)

$$A = 4g^2\sqrt{\frac{3}{\pi M}}\frac{\mathcal{R}'(0)}{M^3} \quad (2.27)$$

which coincides with the normalization of the vertex obtained within the QMRK approach (2.24).

In the leading order, therefore, the QMRK approach is in agreement with the KMR approach in the limit of large meson mass $M \gg |\mathbf{q}_{1,t}|, |\mathbf{q}_{2,t}|$. We shall discuss deviations from this approximation due to the off shell effects in Sec. V. A similar analysis of the off shell effects was performed recently for inclusive Higgs production in Ref. [42].

D. Off-diagonal UGDFs in the general case

The calculation of the amplitude requires the use of the off-diagonal unintegrated gluon distributions. At present these objects are rather poorly known.

While in the KMR approach [1] there is a reasonable prescription how to estimate the off-diagonal UGDFs, there is no unique procedure in the general case. In our case of (relatively light) $\chi_c(0)$ production one is sensitive to rather small transverse momenta of gluons. This is clearly a nonperturbative region where the KMR approach cannot be used directly.

We propose to use the following procedure interpolating between the usual (diagonal) unintegrated gluon distributions:

$$f^{\rm off}_{g,1} = \sqrt{f^{(1)}_g(x_1', q^2_{0,t})\cdot f^{(1)}_g(x_1, q^2_{1,t})}\cdot F_1(t_1), \qquad f^{\rm off}_{g,2} = \sqrt{f^{(2)}_g(x_2', q^2_{0,t})\cdot f^{(2)}_g(x_2, q^2_{2,t})}\cdot F_1(t_2), \quad (2.28)$$

where $F_1(t_1)$ and $F_1(t_2)$ are isoscalar nucleon form factors [43]

$$F_1(t_{1,2}) = \frac{4m_p^2 - 2.79t_{1,2}}{(4m_p^2 - t_{1,2})(1 - t_{1,2}/071)^2}, \quad (2.29)$$

and t_1 and t_2 are total four-momentum transfers in the first and second proton line, respectively. The proton form factor in the form (2.29) gives a rather good description of the t dependence of an elastic pp cross section at high energies, i.e., for kinematics similar as in our case.

The prescription for UGDFs (2.28) is a bit arbitrary, although it is inspired by the positivity constraints for the *collinear* generalized parton distributions [44]. It provides, however, an interpolation between different x and q_t^2 values. A future theoretical work is clearly needed. By construction, in the case $x_1 = x_1'$, $\vec{q}_{0t} = -\vec{q}_{1t}$ or $x_2 = x_2'$, $\vec{q}_{0t} = -\vec{q}_{2t}$ the off-diagonal distributions become the standard diagonal distributions. Such a prescription is more symmetric in variables of the first and second gluon exchanges than the one used in Ref. [45] for Higgs boson production.

In the present work, we shall use a few sets of unintegrated gluon distributions which aim at the description of phenomena where small gluon transverse momenta are involved. Some details concerning these distributions can be found in Ref. [46]. We shall follow the notations there.

The larger energies become, the smaller values of parton momentum fractions come into the game. Therefore at larger energies we shall use distributions constructed exclusively for small values of x. Two of them are based on the idea of gluon saturation. The first of them was obtained based on a saturation-inspired parametrization of the dipole-nucleon cross section that leads to a good description of the HERA data [47]. The second one [48] was constructed to describe the inclusive RHIC pion spectra. The third one is the asymptotic BFKL distribution [49]. It

is considered only for illustration. The asymptotic BFKL UGDF should be taken with some caution, because the corresponding theoretical structure function does not describe the HERA data. Further details may be found in individual references as well as in Ref. [46] where applications of UGDFs to $c\bar{c}$ correlations were discussed.

Because of its simplicity the Gaussian smearing of initial transverse momenta is a good reference point for other approaches. It allows one to study phenomenologically the role of transverse momenta in several high-energy processes. We define simple unintegrated gluon distribution

$$\mathcal{F}_g^{\text{Gauss}}(x, k_t^2, \mu_F^2) = xg^{\text{coll}}(x, \mu_F^2) \cdot f_{\text{Gauss}}(k_t^2), \qquad (2.30)$$

where $g^{\text{coll}}(x, \mu_F^2)$ are standard collinear (integrated) gluon distribution and $f_{\text{Gauss}}(k_t^2)$ is a Gaussian two-dimensional function

$$f_{\text{Gauss}}(k_t^2) = \frac{1}{2\pi\sigma_0^2} \exp(-k_t^2/2\sigma_0^2)/\pi. \qquad (2.31)$$

The UGDF defined by Eq. (2.30) is normalized such that

$$\int \mathcal{F}_g^{\text{Gauss}}(x, k_t^2, \mu_F^2) dk_t^2 = xg^{\text{coll}}(x, \mu_F^2). \qquad (2.32)$$

The UGDFs have the following property

$$f(x, k_t^2) \to 0, \qquad (2.33)$$

if $k_t^2 \to 0$. The small-k_t^2 region is of nonperturbative nature and is rather modeled than derived from pQCD.

The (x, k_t^2, μ^2)-dependent off-diagonal distributions require a separate discussion. It seems reasonable, at least in the first approximation, to take

$$f_{g,1}^{\text{off}} = \sqrt{f_g^{(1)}(x_1', q_{0,t}^2, \mu_0^2) \cdot f_g^{(1)}(x_1, q_{1,t}^2, \mu^2)} \cdot F_1(t_1),$$
$$f_{g,2}^{\text{off}} = \sqrt{f_g^{(2)}(x_2', q_{0,t}^2, \mu_0^2) \cdot f_g^{(2)}(x_2, q_{2,t}^2, \mu^2)} \cdot F_1(t_2). \qquad (2.34)$$

The choice of the (factorization) scales here is not completely obvious either. We shall try the following three choices:

$$\text{(1) } \mu_0^2 = M^2, \qquad \mu^2 = M^2,$$
$$\text{(2) } \mu_0^2 = Q_0^2, \qquad \mu^2 = M^2,$$
$$\text{(3) } \mu_0^2 = q_{0,t}^2 (+ \text{ freezing at } q_{0,t}^2 < Q_0^2), \qquad \mu^2 = M^2. \qquad (2.35)$$

The first choice is similar as in Refs. [1,50]. However, it is not obvious if the scale associated with the "hard" production ($g^*g^* \to \chi_c$) can be used for the left part of the gluonic ladder where no obvious hard scale appears. Therefore we shall try also the second choice where we shall use $Q_0^2 = 0.26$ GeV^2, i.e., the nonperturbative input for the QCD evolution in Ref. [39]. Another option was proposed by Lonnblad and Sjödahl in Ref. [15]. They take $q_{0,t}^2$ as a first scale. In our case, this prescription has to be supplemented by freezing the scale for gluon transverse momenta smaller than Q_0 (minimal perturbative scale).

When inspecting Eqs. (2.5) and (2.28) it becomes clear that the cross section for elastic double-diffractive production of a meson is much more sensitive to the choice of UGDFs than the inclusive cross sections.

III. $\gamma^*\gamma^*$ FUSION MECHANISM

As stated in the introduction we wish to investigate the competition of the diffractive QCD mechanism discussed in the previous sections and the $\gamma^*\gamma^*$-fusion mechanism shown in more detail in Fig. 8.

A. NRQCD approach

In the region of large energies ($\sqrt{s} \gg M + 2m_N$) and small momenta transfer $t_{1,2}$ ($|t_{1,2}| \ll 4m_N^2$) the matrix element for $pp \to pp\chi_{cJ}$ reaction via $\gamma^*\gamma^*$ fusion can be written as [29]

$$\mathcal{M}^{\gamma^*\gamma^*} \approx eF_1(t_1) \frac{(p_1 + p_1')^\nu}{t_1} V_{\mu\nu}^{\gamma^*\gamma^* \to \chi_{cJ}}(q_1, q_2) \times \frac{(p_2 + p_2')^\mu}{t_2} eF_1(t_2), \qquad (3.1)$$

where $F_1(t_1)$ and $F_1(t_2)$ are Dirac proton electromagnetic form factors, and the $\gamma^*\gamma^* \to \chi_{cJ}$ vertex has analogous form as (2.10)

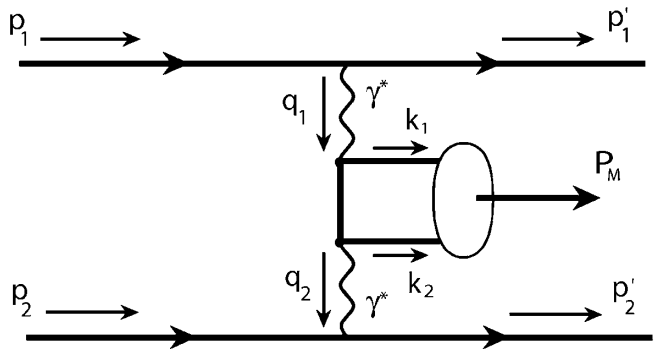

FIG. 8. Kinematics of exclusive $\gamma^*\gamma^*$ fusion mechanism of χ_c-meson production.

$$V^{\gamma^*\gamma^*\to\chi_{cJ}}_{\mu\nu}(q_1,q_2) = \mathcal{P}(q\bar{q}\to\chi_{cJ}) \bullet \Psi_{\mu\nu}(k_1,k_2)$$
$$= 2\pi\cdot\sum_{i,k}\sum_{L_z,S_z}\frac{1}{\sqrt{m}}\int\frac{d^4q}{(2\pi)^4}\delta\left(q^0-\frac{\mathbf{q}^2}{M}\right)$$
$$\times\times\Phi_{L=1,L_z}(\mathbf{q})\cdot\langle L=1,L_z;S=1,S_z|J,J_z\rangle\langle 3i,\bar{3}k|1\rangle\,\mathrm{Tr}\{\Psi^{ik}_{\mu\nu}\mathcal{P}_{S=1,S_z}\},$$
$$\Psi^{ik}_{\mu\nu} = \delta^{ik}\left(\frac{2e}{3}\right)^2\left[\gamma_\nu\frac{\hat{q}_1-\hat{k}_1+m}{(q_1-k_1)^2-m^2}\gamma_\mu-\gamma_\mu\frac{\hat{q}_1-\hat{k}_2+m}{(q_1-k_2)^2-m^2}\gamma_\nu\right],$$
$$\langle 3i,\bar{3}k|1\rangle = \frac{\delta^{ik}}{\sqrt{N_c}}, \tag{3.2}$$

and $\delta^{ik}\delta_{ik}=N_c$.

In the case of scalar meson ($J=0$) the resulting amplitude can be rewritten in the general gauge invariant form [42] in terms of two independent form factors

$$V^{\gamma^*\gamma^*\to\chi_{c0}}_{\mu\nu}(q_1,q_2) = -4i\left(\frac{2e}{3}\right)^2\frac{\mathcal{R}'(0)}{M}\sqrt{\frac{N_c}{\pi M}}\{F_1(q_1,q_2)$$
$$\times((q_1q_2)g_{\mu\nu}-q_{1,\mu}q_{2,\nu})$$
$$+F_2(q_1,q_2)\Big(q_{1,\nu}q_{2,\mu}$$
$$-\frac{q_1^2}{(q_1q_2)}q_{2,\mu}q_{2,\nu}-\frac{q_2^2}{(q_1q_2)}q_{1,\mu}q_{1,\nu}$$
$$+\frac{q_1^2q_2^2}{(q_1q_2)^2}q_{1,\mu}q_{2,\nu}\Big)\Big\}, \tag{3.3}$$

where

$$F_1(q_1,q_2) = \frac{q_1^2q_2^2+(q_1q_2)(q_1^2+q_2^2-3(q_1q_2))}{(q_1q_2)^3},$$
$$F_2(q_1,q_2) = \frac{1}{(q_1q_2)}.$$

In analogy to the diffractive case (2.3) let us define the photon transverse momenta. Momentum conservation dictates us the following decompositions of the photon momenta into the longitudinal and transverse parts

$$q_1 = x_1p_1+\frac{t_1}{s}p_2+q_{1,t},$$
$$q_2 = -x_2p_2-\frac{t_2}{s}p_1+q_{2,t},\qquad q^2_{1/2,t}\simeq t_{1,2}(1-x_{1,2}), \tag{3.4}$$

where $t_{1,2}\equiv q^2_{1,2}$. Because of gauge invariance we have [similarly to (2.9)]

$$(p_1+p_1')^\nu V_{\mu\nu}(p_2+p_2')^\mu = 4p_1^\nu p_2^\mu V_{\mu\nu}. \tag{3.5}$$

In the relevant limit $t_{1,2}\ll x_{1,2}s$ we finally get the following matrix element for $pp\to ppX_c(0)$ reaction via $\gamma^*\gamma^*$ fusion

$$\mathcal{M}^{\gamma^*\gamma^*} \approx -i4s\left(\frac{4e^2}{3}\right)^2\frac{\mathcal{R}'(0)}{M}\sqrt{\frac{N_c}{\pi M}}\frac{F_1(t_1)}{t_1}\frac{F_1(t_2)}{t_2}$$
$$\times\frac{3M^2(q_{1,t}q_{2,t})+2t_1t_2-(q_{1,t}q_{2,t})(t_1+t_2)}{(M^2-t_1-t_2)^2}, \tag{3.6}$$

where $(q_{1,t}q_{2,t}) = -\sqrt{t_1t_2(1-x_1)(1-x_2)}\cos\Phi$, and Φ is the relative angle between photons (or outgoing protons). The amplitude (3.6) is purely imaginary, so there is no interference with diffractive process described by a purely real amplitude (2.5). This amplitude will be used in the following to calculate the differential cross section.

B. Equivalent photon approximation

In the equivalent photon approximation (EPA) the total cross section for $pp\to p\chi_c(0)p$ can be written as a convolution of the EPA flux factors and the $\gamma\gamma\to\chi_c(0)$ resonant cross section

$$\sigma = \int dz_1dz_2\left(\frac{dn}{dz_1}(z_1)\frac{dn}{dz_2}(z_2)\sigma(\gamma\gamma\to\chi_c(0))\right). \tag{3.7}$$

The elementary cross section can be written in terms of partial decay width as

$$\sigma(\gamma\gamma\to\chi_c(0)) \approx \frac{4\pi^2}{M_R^2}\Gamma_{\chi_c(0)\to\gamma\gamma}\delta(M-M_R). \tag{3.8}$$

Let us introduce two new variables,

$$x_F = z_1-z_2\qquad M=\sqrt{sz_1z_2}. \tag{3.9}$$

Now the cross section can be written as

$$\frac{d\sigma}{dx_FdM} = \frac{2M}{s(z_1+z_2)}\frac{dn}{dz_1}(z_1)\frac{dn}{dz_2}(z_2)\frac{4\pi^2}{M_R^2}$$
$$\times\Gamma_{\chi_c(0)\to\gamma\gamma}\delta(M-M_R). \tag{3.10}$$

Integrating over invariant mass of the two photons we get

$$\frac{d\sigma}{dx_F} = \frac{2M_R}{s(z_1+z_2)}\frac{dn}{dz_1}(z_1)\frac{dn}{dz_2}(z_2)\frac{4\pi^2}{M_R^2}\Gamma_{\chi_c(0)\to\gamma\gamma}, \tag{3.11}$$

where

$$z_1 = \tfrac{1}{2}x_F + \tfrac{1}{2}\sqrt{x_F^2 + 4M_R^2/s},$$
$$z_2 = -\tfrac{1}{2}x_F + \tfrac{1}{2}\sqrt{x_F^2 + 4M_R^2/s}. \quad (3.12)$$

This equation is suitable to calculate distribution of $\chi_c(0)$ in the Feynman variable x_F. The analytical flux factors of photons in protons of Drees and Zeppenfeld [51] are taken. We have also tried

$$f(z) \equiv \frac{dn}{dz}(z) = \int d^2q_t \frac{q_t^2}{(q_t^2 + z^2 m_N^2)^2} F_1^2(t), \quad (3.13)$$

where $t = -(q_t^2 + z m_N^2)/(1-z)$. The decay width from the Particle Data Group [52] is $\Gamma_{\chi_c(0)\to\gamma\gamma} = 0.2626 \cdot 10^{-5}$ GeV.

IV. POMERON-POMERON FUSION

We have shown above how to calculate the diffractive $\chi_c(0^+)$ meson production mechanism in a QCD-inspired approach. In order to describe the high-energy processes, in the literature one uses often a phenomenological object known as Pomeron. Such an object is often assigned a vector nature, i.e., it is assumed that it couples to the nucleons or (quarks) via γ_μ matrices, i.e., similarly as photon. The corresponding mechanism for the exclusive χ_c meson production is sketched in Fig. 9.

The amplitude for the exclusive process considered may be written as

$$\mathcal{M}^{\mathbb{PP}\to\chi_{cJ}}_{pp\to pp\chi_{cJ}} \approx A_R(s_1,t_1)(p_1 + p_1')^\nu V^{\mathbb{PP}\to\chi_{cJ}}_{\mu\nu}(q_1,q_2) \times (p_2 + p_2')^\mu A_R(s_2,t_2). \quad (4.1)$$

In the equation above $A_R(s_{1/2},t_{1/2})$ are so-called Regge propagators. They can be written as

$$A_R(s_{1/2},t_{1/2}) = r_c \frac{C_{\mathbb{P}}}{3}\left(\frac{s_{1/2}}{s_0}\right)^\delta F_1^{\mathbb{P}}(t_{1/2}). \quad (4.2)$$

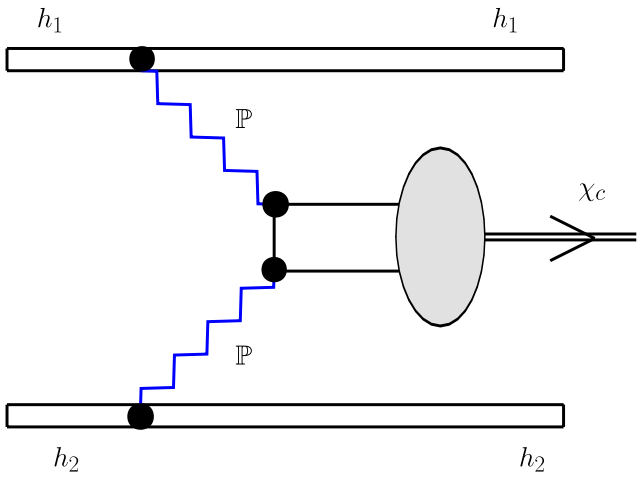

FIG. 9 (color online). Pomeron-Pomeron fusion mechanism of χ_c-meson production.

$F_1^{\mathbb{P}}(t_{1/2})$ is a form factor describing the helicity-preserving coupling of the Pomeron to the nucleon. We take F_1 to be identical to the Dirac electromagnetic form factors of the proton. Such a choice is justified by the phenomenology of elastic proton-proton scattering (see, e.g., [43]). The Pomeron coupling to the charm quark and/or antiquark is reduced when compared to the coupling to the nucleon ($C_{\mathbb{P}}$) by a factor of 3 (three quarks in the nucleon versus single charm quark/antiquark) and an extra factor r_c (heavy quark interaction is weaker than light quark interaction). This parameter can be extracted from the inelastic interaction of J/ψ with the nucleons in nuclei [21]. At the Tevatron energy $r_c \sim 0.2$. The parameters of the Pomeron exchanges, $C_{\mathbb{P}}$ and δ are taken from the Donnachie-Landshoff fits to the proton-proton and proton-antiproton total cross sections [53]. The vertex $V^{\mathbb{PP}\to\chi_c}$ can be obtained from the vertex $V^{\gamma^*\gamma^*\to\chi_c}$ by replacing charm quark charge by unity.

The comparison of the results for the Pomeron-Pomeron fusion with the diffractive QCD results will be given in the next section.

V. RESULTS

In Ref. [21] the estimates of the integrated cross sections were given. We wish to concentrate here on the differential distributions. Before we show our results, we wish to discuss the uncertainties related to the KMR approach.

A. Uncertainties in the KMR approach

In the KMR approach only one effective transverse momentum is taken explicitly in their skewed unintegrated distributions. In the KMR prescription it is the minimum of the transverse momenta of the two gluons connected to the same proton line. In order to see the uncertainties related to such a choice we shall present results obtained with the following, equally arbitrary, choices:

(1) $Q_{1,t}^2 = \min(q_{0,t}^2, q_{1,t}^2)$, $Q_{2,t}^2 = \min(q_{0,t}^2, q_{2,t}^2)$.
(2) $Q_{1,t}^2 = \max(q_{0,t}^2, q_{1,t}^2)$, $Q_{2,t}^2 = \max(q_{0,t}^2, q_{2,t}^2)$.
(3) $Q_{1,t}^2 = q_{1,t}^2$, $Q_{2,t}^2 = q_{2,t}^2$.
(4) $Q_{1,t}^2 = q_{0,t}^2$, $Q_{2,t}^2 = q_{0,t}^2$.
(5) $Q_{1,t}^2 = (q_{0,t}^2 + q_{1,t}^2)/2$, $Q_{2,t}^2 = (q_{0,t}^2 + q_{2,t}^2)/2$.

As an example, in Fig. 10 we show results for the Feynman x_F distribution. As can be seen from the figure there are rather large uncertainties related to the choice of the effective transverse momentum.

The estimate by Khoze, Martin, Ryskin, and Stirling in Ref. [21] was done for one selected value of the hard scale in the KMR UGDF $\mu^2 = M_{\chi_c(0)}^2/4$. In Fig. 11 we show the dependence of the differential cross section on the value of the scale. There is a sizeable effect (about a factor of 2) on the cross section (see also Table I with integrated cross sections). For $x_F \sim 0$, the smaller μ^2, the bigger the cross section.

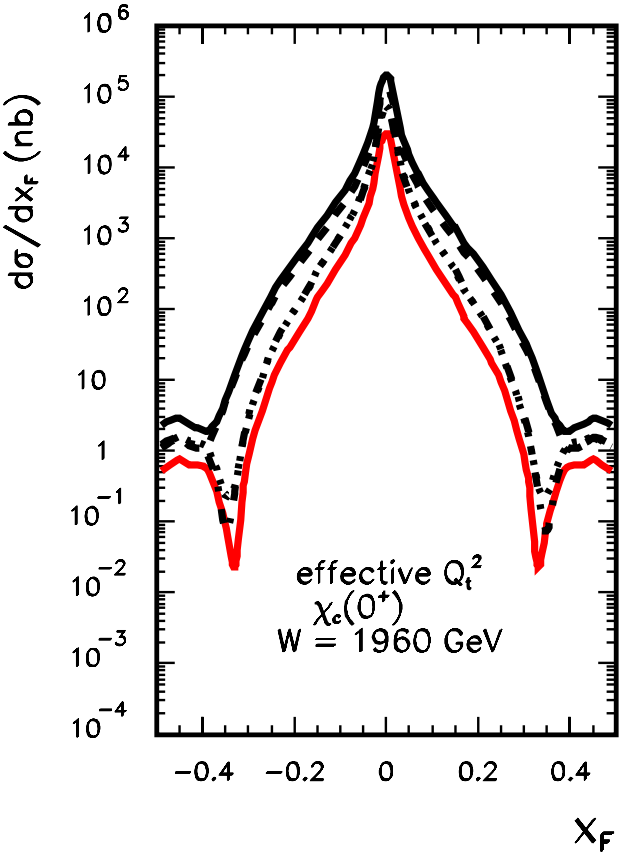

FIG. 10 (color online). Dependence of the distribution in Feynman variable x_F on the effective transverse momentum in the KMR approach. The solid lines are choice 1 (upper line) and choice 2 (lower line), the dashed line is choice 3, the dotted line is choice 4, and the dash-dotted line is choice 5. The calculation was done for Tevatron energy $W = 1960$ GeV.

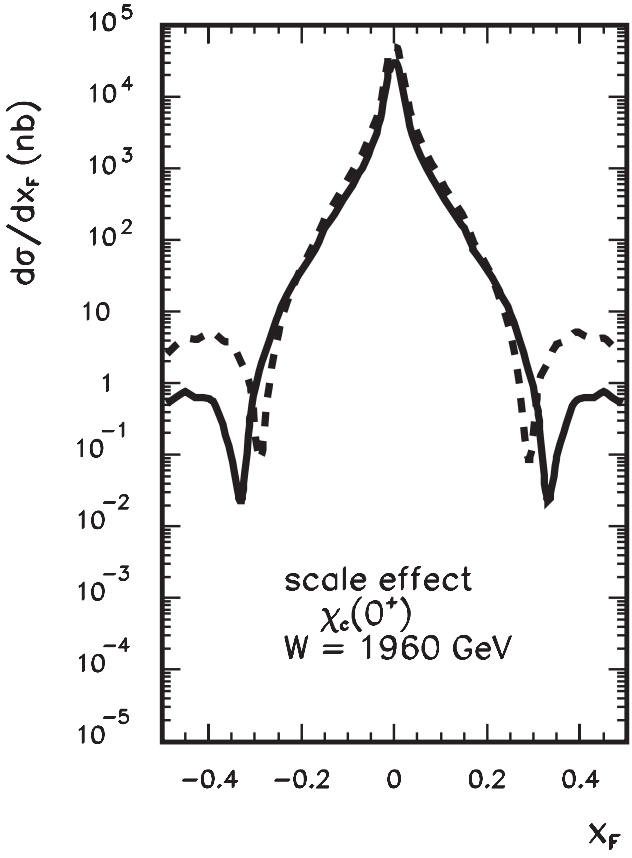

FIG. 11. Scale effect on distribution in Feynman x_F in the KMR approach (KMR UGDF, KMR vertex). The solid line is $\mu^2 = M_\chi^2$. The dashed line is $\mu^2 = M_\chi^2/4$. The calculation was done for Tevatron energy $W = 1960$ GeV.

TABLE I. Integrated cross section (in nb) for exclusive $\chi_c(0^+)$ production for Tevatron energy $W = 1960$ GeV in various possible theoretical prescriptions. The numbers for Gaussian UGDF refer to prescription in Eq. (2.35). The number in brackets means a power of 10.

UGDF, details	$\sigma_{\rm tot}$	$S^2\sigma_{\rm tot}$	$\mathrm{BR}S^2\sigma_{\rm tot}$
1. KMR, $Q_{\rm cut}^2 = 0.26$ GeV^2, on shell vertex, min. prescription for Q_t^2	0.1357(+4)	0.1357(+3)	0.1357(+1)
2. KMR, $Q_{\rm cut}^2 = 0.26$ GeV^2, on shell vertex, max. prescription for Q_t^2	0.8585(+4)	0.8585(+3)	0.8585(+1)
3. KMR, $Q_{\rm cut}^2 = 0.26$ GeV^2, off shell vertex, min. prescription for Q_t^2	0.3723(+3)	0.3723(+2)	0.3723(+0)
4. KMR, $Q_{\rm cut}^2 = 0.5$ GeV^2, on shell vertex, min. prescription for Q_t^2	0.8227(+3)	0.8227(+2)	0.8227(+0)
5. KMR, $Q_{\rm cut}^2 = 0.8$ GeV^2, on shell vertex, min. prescription for Q_t^2	0.4124(+3)	0.4124(+2)	0.4124(+0)
6. KMR, $Q_{\rm cut}^2 = 1.0$ GeV^2, on shell vertex, min. prescription for Q_t^2	0.2745(+3)	0.2745(+2)	0.2745(+0)
4. KL, on shell vertex	0.1180(+3)	0.1180(+2)	0.1180(+0)
5. KL, off shell vertex	0.5231(+2)	0.5231(+1)	0.5231(−1)
6. GBW, on shell vertex	0.8514(+2)	0.8514(+1)	0.8514(−1)
7. GBW, off shell vertex	0.6636(+2)	0.6636(+1)	0.6636(−1)
8. BFKL, on shell vertex	0.2603(+4)	0.2603(+3)	0.2603(+1)
9. BFKL, off shell vertex	0.1125(+4)	0.1125(+3)	0.1125(+1)
10. Gauss, $\sigma_0 = 0.5$ GeV, off shell vertex, scales (2)	0.2141(+2)	0.2141(+1)	0.2141(−1)
11. Gauss, $\sigma_0 = 1.0$ GeV, off shell vertex, scales (2)	0.1811(+1)	0.1811(+0)	0.1811(−2)

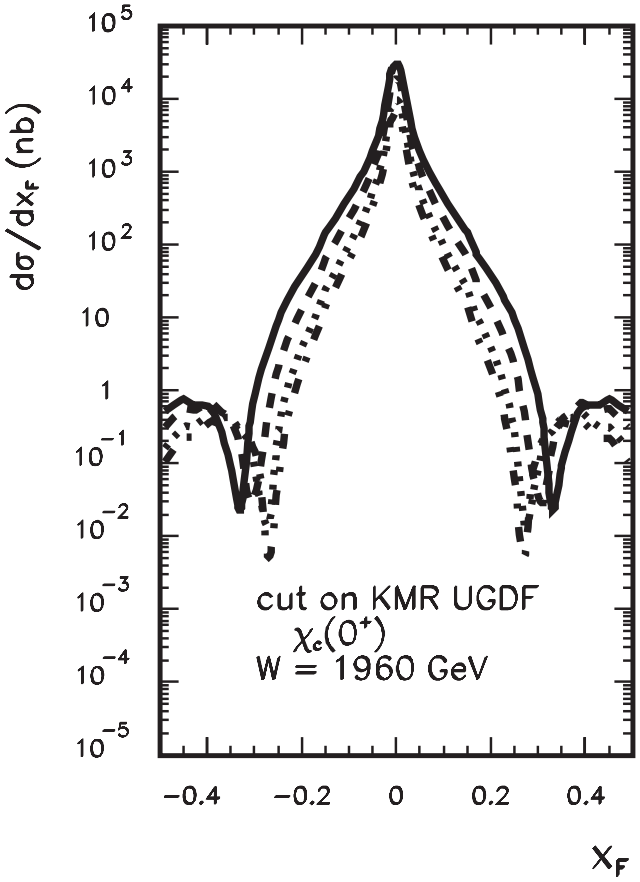

FIG. 12. Dependence of distribution in Feynman x_F in the KMR approach (KMR UGDF, KMR vertex) on the lower cut on the gluon transverse momenta on distribution in Feynman x_F in the KMR approach. The solid line is for $Q^2_{\rm cut} = 0.26$ GeV^2, the dashed line for $Q^2_{\rm cut} = 0.5$ GeV^2, the dotted line for $Q^2_{\rm cut} = 0.8$ GeV^2, and the dash-dotted line for $Q^2_{\rm cut} = 1.0$ GeV^2. The calculation was done for the Tevatron energy $W = 1960$ GeV.

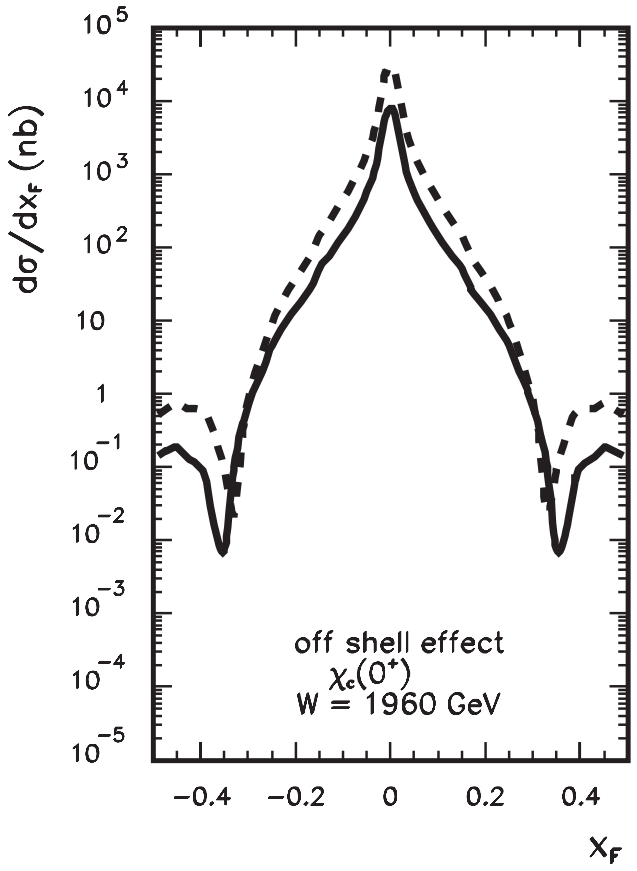

FIG. 13. Off shell effect on distribution in Feynman x_F in the KMR approach. The dashed line is the on shell case. The solid line is the off shell case. The calculation was done for the Tevatron energy $W = 1960$ GeV.

In order to demonstrate the sensitivity to the nonperturbative region of small transverse momenta in Fig. 12 we show results with the KMR UGDF cutoff for small values of the effective gluon transverse momenta $Q_t^2 > Q^2_{\rm cut}$. One observes a rather strong dependence on the value of the cutoff parameter. The bigger the value of the cutoff parameter, the smaller the cross section. The results for the integrated cross section are summarized in Table I. Even for large values of the cutoff parameter ($Q^2_{\rm cut} \sim 1$ GeV^2) sizeable cross sections are obtained.

The estimate in Ref. [21] was done assuming that the gluons in the $gg \to \chi_c(0^+)$ vertex are on mass shell, which is exact only in the infinite meson mass limit. In this paper (see, subsection II B), we take into account the effect of gluon virtualities. In Fig. 13 we show the role of the off shell effects for the KMR UGDF. The off shell effect leads to a reduction of the cross section by a factor of 2–5.

Finally, in Fig. 14 we show the influence of the off shell effects on the azimuthal-angle correlation function. The off shell effect in the matrix element reduces the cross section but does not change its shape. The shape of the distribution requires an extra comment. The distribution in the azimuthal angle is very different from $(1 + \cos(2\Phi))$ expected for a one-step vector-vector fusion (e.g., photon-photon, Pomeron-Pomeron fusion) to be discussed in detail in the next subsection.

In many applications of the k_t^2-factorization approach, the use of gluon virtualities instead of a large scale given by a ''massive'' object(s) produced in the final state enhances cross section. In Fig. 15 we show how the results change if the strong coupling constants $g_s(M_\chi^2)g_s(M_\chi^2)$ in the vertex $g^*g^* \to \chi_c(0^+)$ are replaced by running coupling constants $g_s(q_{1t}^2)g_s(q_{2t}^2)$, where $-q_{1t}^2$ and $-q_{2t}^2$ are virtualities of the gluons entering the vertex. Since in the case of relatively light (compared to Higgs boson) $\chi_c(0^+)$ the dominant contribution to the amplitude comes from the infrared region, it is not surprising that the results shown in Fig. 15 depend so strongly on the model of α_s in the infrared region. We show results for a few representative models from the literature. In general, the cross section with α_s running with gluon virtualities is much bigger than that with $\alpha_s(M_\chi^2)$. The Shirkov-Solovtsov model (dashed line) gives

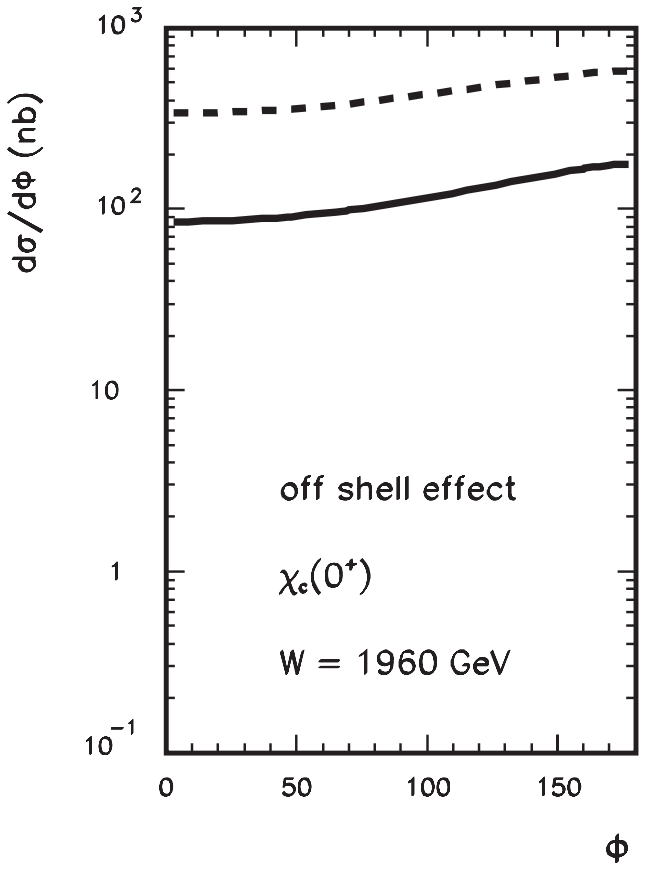

FIG. 14. Off shell effect on distribution on azimuthal correlation function in the KMR approach. The dashed line is the on shell case. The solid line is the off shell case. The calculation was done for the Tevatron energy $W = 1960$ GeV.

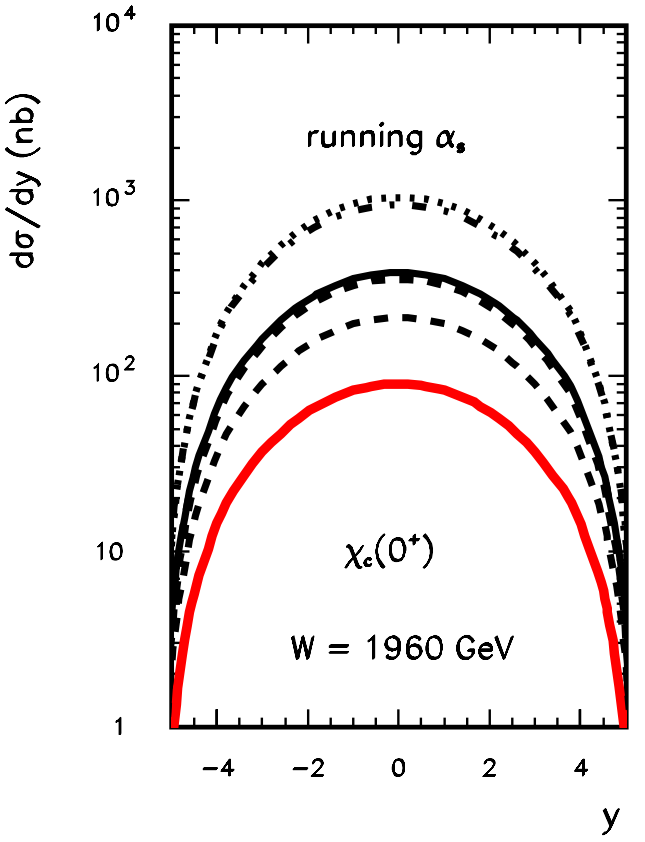

FIG. 15 (color online). $d\sigma/dy$ for different choices of α_s: (a) fixed coupling (thick solid line), (b) Shirkov-Solovtsov (dashed line), (c) parametrization with gluon mass (thick dashed line), (d) Dokshitzer-Khoze-Troyan (dotted line), (e) Alekseev-Arbuzov (dash-dotted line), (f) Webber (thin solid line). In this calculation the KMR UGDFs were used for illustration.

the cross section which is only factor of 2 bigger than that for the fixed coupling constant (thick solid line). The other models give much larger cross sections. A particularly large cross section is obtained with the Dokshitzer-Khoze-Troyan and Alekseev-Arbuzov parametrizations despite that the two models have very different behavior for $k_t^2 \to 0$: in the case of Dokshitzer-Khoze-Troyan $\alpha_s(0) = 0$, while in the case of Alekseev-Arbuzov $\alpha_s(0) = \infty$.

In our opinion, the choice of the renormalization scales $\mu_1^2 = q_{1t}^2$ and $\mu_2^2 = q_{2t}^2$, although often used in the k_t-factorization approaches, has no profound justification. In general, one should rather take $\mu_1^2 = \max(M_\chi^2, q_{1t}^2)$, $\mu_2^2 = \max(M_\chi^2, q_{2t}^2)$. For the exclusive process considered here almost always $q_{1t}^2 < M_\chi^2$ and $q_{2t}^2 < M_\chi^2$. Therefore we think that the choice $\mu_1^2 = M_\chi^2$ and $\mu_2^2 = M_\chi^2$ is better justified and this will be used in the following.

B. Double-diffractive $\chi_c(0^+)$ production within QMRK approach

In Fig. 16 we present differential distributions of the $\chi_c(0^+)$ mesons in the Feynman variable x_F. We present results obtained with different UGDFs. As is characteristic for central diffractive production, all distributions peak at $x_F \approx 0$. Although all UGDFs give similar quality description of the low-x HERA data for the F_2 structure function, they give quite different longitudinal momentum distributions of $\chi_c(0^+)$ at the Tevatron energy $W = 1960$ GeV. The UGDFs which take into account saturation effects [Golec-Biernat-Wusthoff (GBW), Kharzeev-Levin (KL)] give a much lower cross section than the BFKL UGDF (dash-dotted line). As in Ref. [29], rather small values of x's in formula (2.5) come into the game here. Therefore the process considered here would help, at least in principle, to constrain the poorly known UGDFs.

Up to now we have presented the distributions in the Feynman variable x_F. Distributions in the rapidity variable are often considered to provide a better representation of the data. In Fig. 17 we show distributions in rapidity for different UGDFs. In this calculation the off shell vertex is used. The solid lines corresponds to the KMR approach for different prescriptions of effective transverse momentum ("minimum prescription")—lower solid curve, ("maximum prescription")—upper solid curve. The shapes as

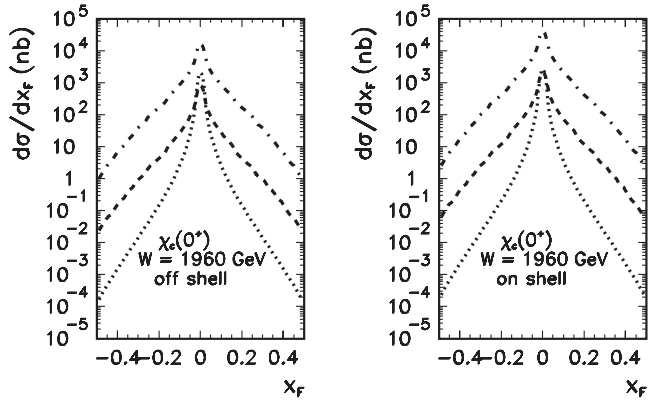

FIG. 16. Distribution in Feynman x_F for different UGDFs (KL–dashed line, GBW–dotted line, BFKL–dash-dotted line) for the off shell (left panel) and on shell (right panel) matrix element. The calculation was done for the Tevatron energy $W = 1960$ GeV.

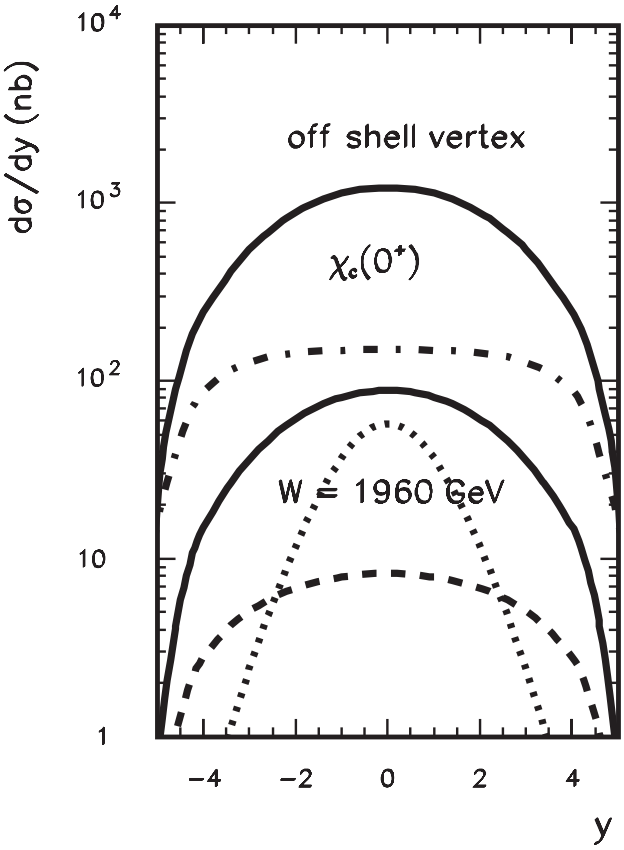

FIG. 17. Rapidity distribution of $\chi_c(0)$ for different unintegrated distributions and the off shell vertex. The meaning of curves is the same as in Fig. 16. Two new solid lines correspond to the KMR UGDFs with minimal (lower curve) and maximal (upper curve) momentum prescription.

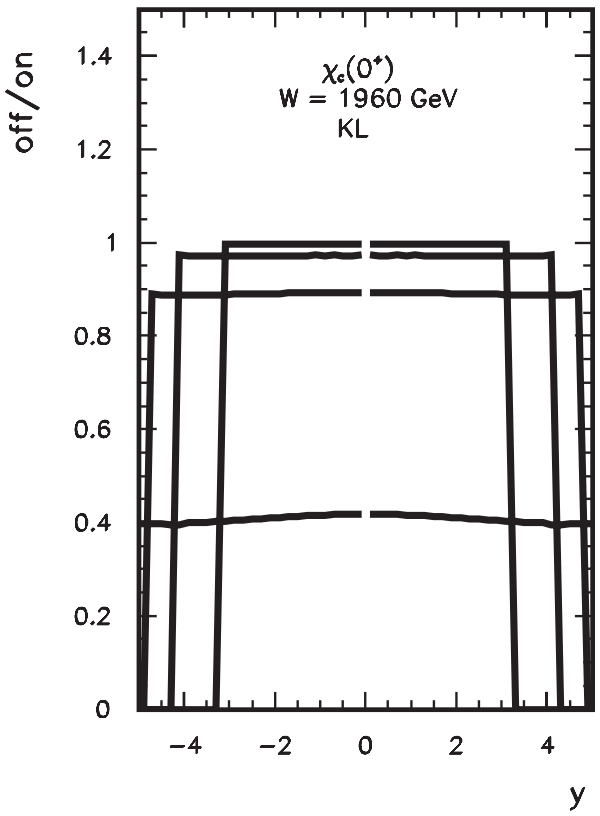

FIG. 18. Ratio of off shell to on shell cross sections as a function of rapidity for different values of meson mass: $M = M_{\chi_c(0)}$, 5, 10, 20 GeV. In this calculation the KL UGDF was used.

well as the size of the cross section depend on the UGDFs. Which distribution is better could, in principle, be verified experimentally. This would require a realistic inclusion of absorptive effect, however. At present there is no agreement on the details of how the latter should be evaluated.

The relatively large off shell effect (compare results in the left and right panel of Fig. 16) requires an extra discussion. In Fig. 18 we show for illustration the ratio of the off shell to the on shell cross sections for the KL UGDF and different arbitrary meson masses. The ratio converges quickly to one with increasing meson mass. Of course, kinematical limits in rapidity become more serious for larger meson mass. For illustration in Fig. 19 we show the ratio of the cross sections for $y = 0$ as a function of the meson mass for two different UGDFs: KL (dashed line) and GBW (dotted line). For small meson mass the ratio depends strongly on UGDF and, in particular, on the distribution in the gluon transverse momenta. The ratio is smaller for distributions that are broader in k_t^2 (compare results obtained with KL and GBW UGDFs).

In Fig. 20 we show distributions in the square of the four-momentum transfers (t_1 or t_2) in the nucleon's lines. Because they are identical we shall denote them $d\sigma/dt$ for brevity. The distributions shown in the figure are

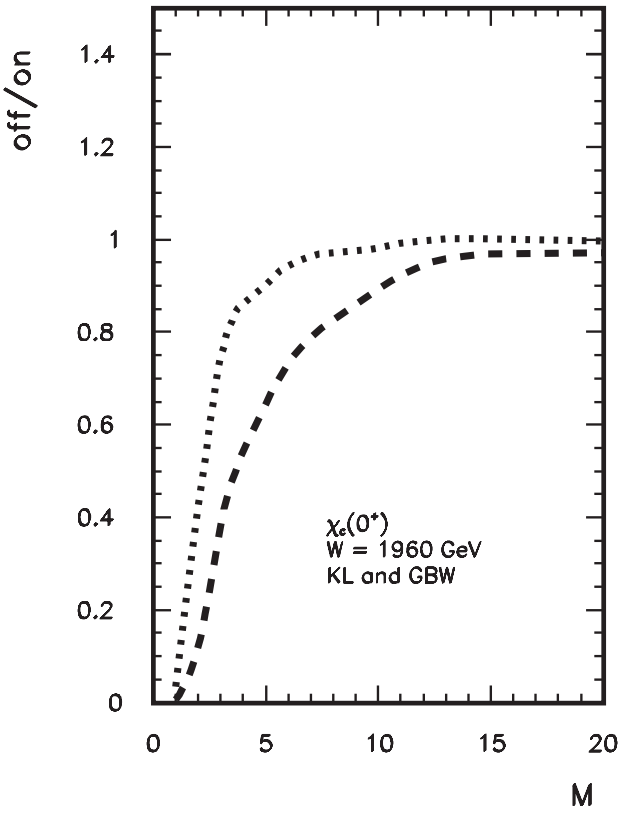

FIG. 19. Ratio of off shell to on shell cross sections as a function of meson mass for $y = 0$ for the KL (dashed line) and GBW (dotted line) UGDFs.

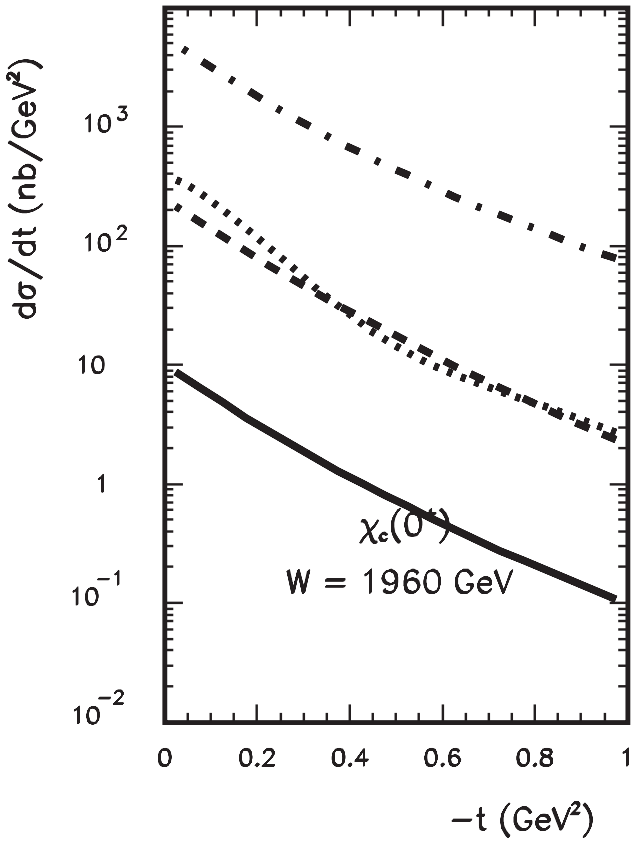

FIG. 20. Distribution in $t = t_1 = t_2$ for different UGDFs. The notation is as in Fig. 16. The solid line corresponds to Gaussian distributions with $\sigma_0 = 1.0$ GeV and the second choice of scales in Eq. (2.35).

peaked at small values of t_1 or t_2. Slightly different slopes are obtained with different UGDFs. This demonstrates how poorly known UGDFs are at present. The measurement of such distributions requires measuring forward protons (or antiprotons). In the case when no measurement of forward nucleons is possible, one should study events with low multiplicity (only particles from the decay of $\chi_c(0^+)$). This can be either pairs of pions or pairs of kaons or pairs of photons or $J/\psi + \gamma$. Unfortunately branching ratios to these channels are rather low [52].

In Fig. 21 we show azimuthal angular correlations of the outgoing nucleons. Measuring such distribution experimentally requires identification of both nucleons in very forward/backward directions. This is not possible with the present Tevatron apparatus. We hope such a measurement will be possible with final LHC instrumentation. All distributions shown in Fig. 21 are peaked at $\Phi \sim 180°$, i.e., for the back-to-back kinematics. The fact that the distributions are not simple functions ($\sin\Phi$, $\cos\Phi$) of the relative azimuthal angle between outgoing nucleons is due to the loop integral in Eq. (2.5) which destroys the dependence one would obtain with single fusion of well-defined objects (mesons or Reggeons).

Another type of proton-antiproton correlation is shown in Fig. 22. The results are for the KL and BFKL UGDFs as well as for the photon-photon fusion. Finally, we show the two-dimensional distribution in t_1 and t_2 for the "fusion" of two vector Pomerons. The (t_1, t_2) distribution obtained in the photon-photon fusion mechanism differs qualitatively from all other distributions. One can see a strong enhancement of the cross section when $t_1 \to 0$ or $t_2 \to 0$. Also the shape of the two-dimensional spectrum obtained for the fusion of phenomenological vector Pomerons differs from those obtained in the QCD-inspired KMR mechanism (please note the minimum of the cross section when $t_1 \to 0$ and/or $t_2 \to 0$).

In order to demonstrate the role of the gluon transverse momenta in UGDFs, in Fig. 23 we show distributions in x_F for the Gaussian UGDF for different values of the smearing parameter σ_0. We would like to notice here that all such UGDFs correspond to identical integrated GDFs. The smaller is the value of σ_0, the larger is the cross section. This demonstrates that the main contributions to the cross section come from the region of very small transverse momenta of the t-channel gluons (see Fig. 4). This is clearly the region where nonperturbative effects are dominant.

Up to now we have concentrated on longitudinal momentum distributions of $\chi_c(0)$ (x_F or y). Transverse mo-

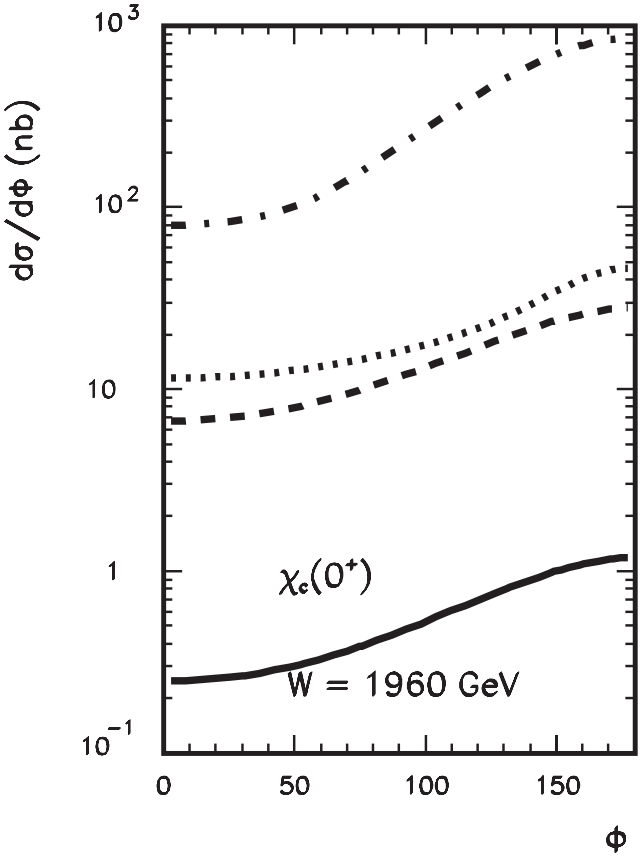

FIG. 21. Distribution in relative azimuthal angle for different UGDFs. The notation is as in Fig. 16. The solid line correspond to Gaussian distribution with $\sigma_0 = 1.0$ GeV and the second choice of scales in Eq. (2.35).

mentum distribution of $\chi_c(0)$ may also be very interesting. Such distributions have never been shown in the literature before. In Fig. 24 we show the distributions at $y = 0$ for the on shell (left panel) and off shell (right panel) matrix elements. Deep minima in the distributions appear in all cases. Both the shapes of distributions and the exact position of the minima depend on the UGDF used. The distribution in p_t is a convolution of the transverse momentum distributions of gluons entering the hard process and would test the latter objects.

The origin of these minima is as follows. The main reason of their appearance is the functional dependence of matrix elements on its arguments. Different kinematical variables can be used as independent variables. In particular, the matrix element can be expressed in terms of the $\chi_c(0)$ rapidity y, the $\chi_c(0)$ transverse momentum p_t, and auxiliary variables $p_{-t,x}$, $p_{-t,y}$, where $\vec{p}_{-t} \equiv \vec{p}'_{1t} - \vec{p}'_{2t}$. Thus the matrix element can be written as $\mathcal{M} = \mathcal{M}(y, p_t, p_{-t,x}, p_{-t,y})$. The maximal contribution to the cross section comes from the region when $p_{-t,x} = p_{-t,y} = 0$. The matrix element changes its sign at a certain, well localized, position in p_t. This position is only weakly dependent on y and on the auxiliary variables $p_{-t,x}$, $p_{-t,y}$. Therefore the position of the cross section minimum coincides with the zero of the matrix element $\mathcal{M}(y = 0, p_t, p_{-t,x} = 0, p_{-t,y} = 0)$. Although it is very interesting, it may be difficult to observe the minima experimentally as it is rather difficult to identify the $\chi_c(0)$ meson. In principle, the following decay channels are of interest: $J/\psi\gamma$, $\pi^+\pi^-$ and K^+K^-. It is not clear to us if such measurements can be realized at the BNL Tevatron.

Let us turn now to the second mechanism of the exclusive $\chi_c(0^+)$ production—the two-photon fusion mechanism sketched in Fig. 2. In Fig. 25 we show the corresponding distribution in the Feynman variable x_F. For comparison we show also the EPA result (dotted line) discussed in Subsec. III B.

For pedagogical purposes, in Fig. 26 we show also the result of calculation with vectorlike Pomerons as described in Sec. IV. Here a rather smaller cross section is obtained when compared to the more QCD-inspired calculation with UGDFs. The cross section depends strongly on the value of parameters of the form factor describing the coupling of the phenomenological Pomeron to nucleons. The value of $B = 15$–20 GeV^{-2} is preferred from the proton-proton or proton-antiproton elastic scattering phenomenology. When compared to the calculation with the UGDFs presented in Fig. 16, the distribution around $x_F = 0$ is much broader here. The thinner distribution in the case of the k_t-factorization approach is due to the x dependence of UGDFs entering the basic formula. The values of x's (x_1, x_2, etc.) in the off-diagonal UGDFs change quickly with Feynman variable x_F which makes the peak at $x_F = 0$ much thinner than for the phenomenological Pomeron exchange discussed here.

Let us return for a while to distributions in t_1 or t_2. In Fig. 27 we show distributions for the photon-photon and phenomenological vector Pomeron—vector Pomeron fusion mechanisms in $t = t_1 = t_2$ (relevant for one-nucleon tagged case) obtained by projecting the two-dimensional distributions shown in Fig. 22. The electromagnetic component peaks at very small values of t due to photon propagators.

The results for the diffractive mechanism depend strongly on the details of the calculation. For easy reference we show only one distribution of the phenomenological (vector-vector fusion) diffractive component here. Although the diffractive component is subjected to much stronger absorption effects than the electromagnetic one, it is clear that the diffractive component dominates.

In Fig. 28 we show differential distribution in the relative azimuthal angle for the $\gamma^*\gamma^*$ and Pomeron-Pomeron fusion mechanisms. One can see a typical $(1 + \cos(2\Phi))$ dependence characteristic for one-step vector exchanges. These distributions are very different from those shown in Fig. 21 for pQCD diffraction where the underlying mechanism is more complicated due to a two-step nature of the process (see Fig. 4).

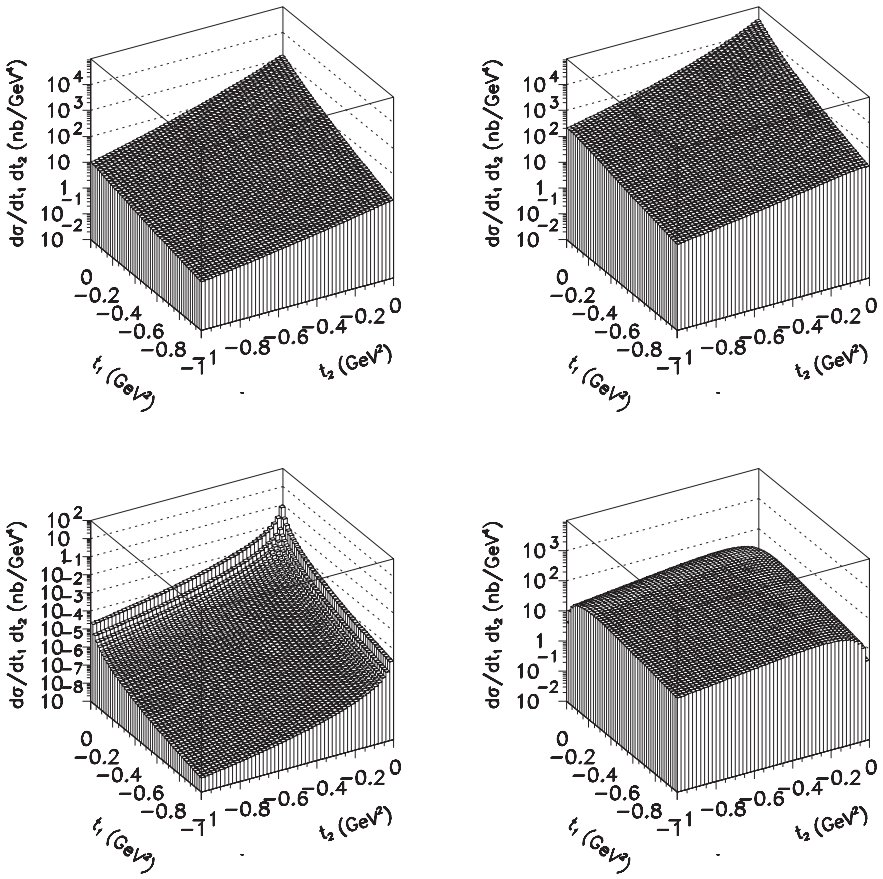

FIG. 22. Two-dimensional maps in t_1 and t_2 for KL UGDF (top left) and BFKL UGDF (top right) as well as for two-photon fusion (bottom left) and two-Pomeron fusion with dipole form factors (bottom right).

Above we have calculated only the bare distributions. They are subject to absorption effects. The absorption effects are usually included by multiplying the bare distributions by a soft gap survival probability. The gap survival probability was estimated to $S^2(\text{Tevatron}) \approx 0.05$ and $S^2(\text{LHC}) \approx 0.025$ [21]. Therefore absorption leads to a large reduction of the bare cross section. In principle, the absorption effects may modify also the shapes of differen-

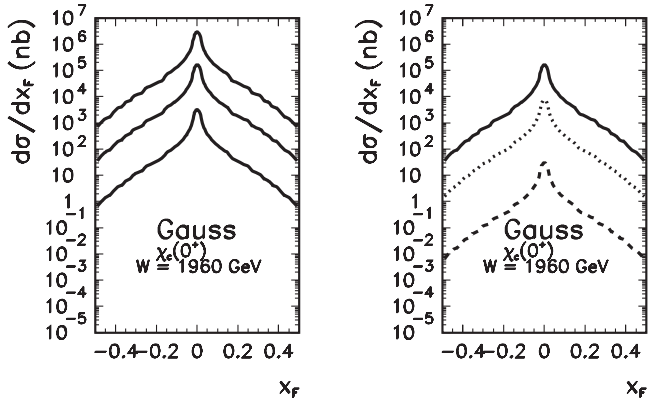

FIG. 23. Distribution in x_F of the $\chi_c(0^+)$ meson for Gaussian UGDF. Left panel: different values of the parameter $\sigma_0 = 0.5$, 1, 2 GeV and $\mu_0^2 = \mu^2 = M_\chi^2$. Right panel: $\sigma_0 = 1$ GeV with different scale choices defined in Eq. (2.35): 1 is the solid line, 2 is the dashed line, and 3 is the dotted line.

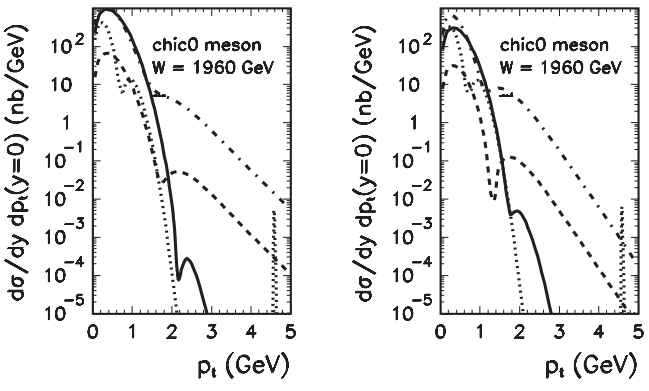

FIG. 24. Transverse momentum distribution of the $\chi_c(0^+)$ meson for $y = 0$ and for different UGDFs. Results with on shell (off shell) matrix elements are shown in the left (right) panel. The meaning of the curves here is as in Fig. 16. The solid line corresponds to the KMR gluon distribution.

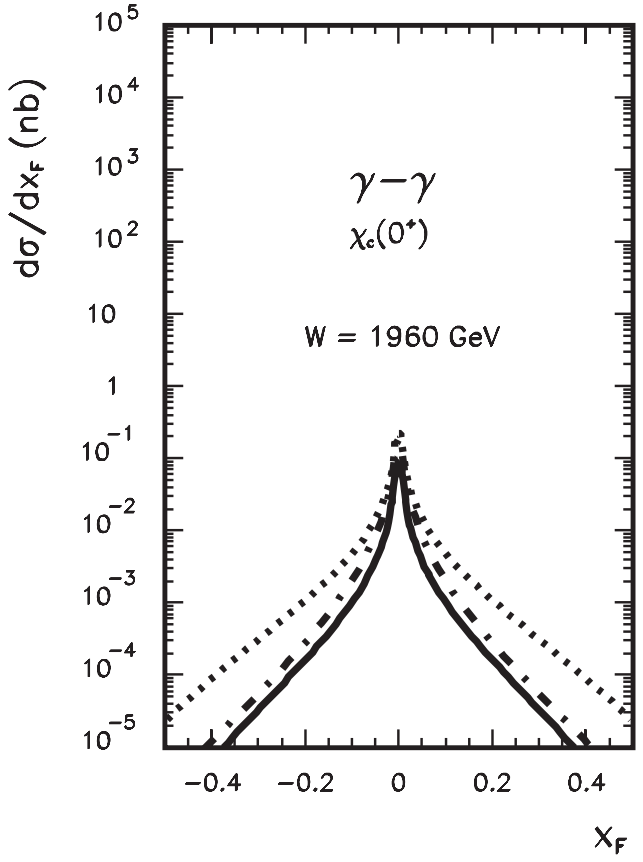

FIG. 25. Distribution in x_F for two-photon fusion. The solid line represents the result obtained with Eq. (3.6). The otted and dashed-dotted lines correspond to the EPA approach with different flux factors as described in the text.

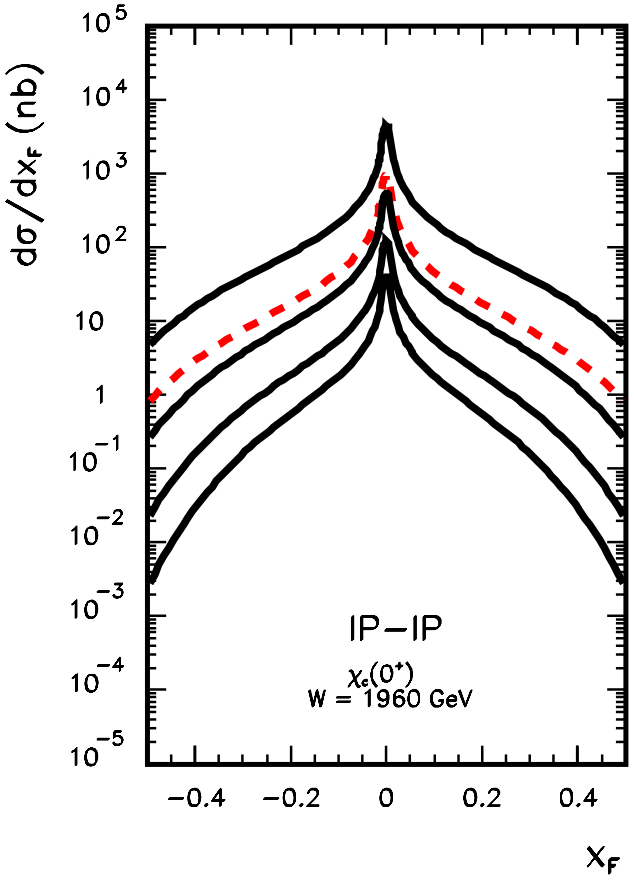

FIG. 26 (color online). Distribution in x_F for two-Pomeron fusion for different values of the slope parameter $B = 5, 10, 15, 20$ GeV^{-2} (from top to bottom) of the exponential form factor. The dashed line is obtained with the dipole (electromagnetic) form factor.

tial distributions. This requires a further detailed analysis which goes beyond the scope of the present paper.

As discussed in this paper, there are huge uncertainties in estimating the cross section for the exclusive $\chi_c(0^+)$ production. They are much larger than, e.g., for the elusive J/ψ production where the corresponding amplitude can be related to the amplitude of J/ψ photoproduction in ep collisions [54]. Only experiments may shed more light on the dynamics of the $\chi_c(0^+)$ production mechanism. Measuring centrally produced $\chi_c(0^+)$, one forward nucleon (proton or antiproton) and imposing the condition of rapidity gap in the second hemisphere should allow, at least in principle, such a measurement.

In Table I we have combined the cross section integrated over the whole available phase space for the exclusive production of the $\chi_c(0^+)$ mesons. In calculations we have assumed $W = 1960$ GeV, $S^2 = 0.1$, and $\mathrm{BR}(\chi_c(0^+) \to J/\psi + \gamma) = 0.01$. The recently measured value of the branching ratio is $1.3 \pm 0.11\%$ [52]. The last column shows a possible contribution of the $\chi_c(0^+) \to J/\psi + \gamma$ decay to the exclusive production of J/ψ if the soft photon cannot be correctly identified. We get typically 0.1–5 nb, i.e., much less than the direct J/ψ photoproduction [54]. It would be interesting to calculate the contribution of $\chi_c(1^+) \to J/\psi\gamma$ and $\chi_c(2^+) \to J/\Psi\gamma$, where the corresponding branching ratios are an order of magnitude larger. On the other hand, within the approximations made in Ref. [20] the cross sections for diffractive production of $\chi_c(1^+)$ and $\chi_c(2^+)$ vanish. It would be interesting to go beyond the approximations of Ref. [20].

The exclusive production of χ_c has been reported recently by the CDF Collaboration [55] with the upper limit for the cross section

$$\sigma_{\mathrm{exc}}(p\bar{p} \to p + J/\psi + \gamma + \bar{p}) < 49 \pm 18(\mathrm{stat}) \pm 39(\mathrm{sys})\ \mathrm{pb}, \tag{5.1}$$

within the CDF experimental cuts. These numbers cannot be directly compared with our results in Table I that do not include the experimental cuts. Such a comparison requires a Monte Carlo type analysis as in Ref. [56] and inclusion of all χ_c states. Some work in this direction is in progress. We expect better and official results of the CDF Collaboration

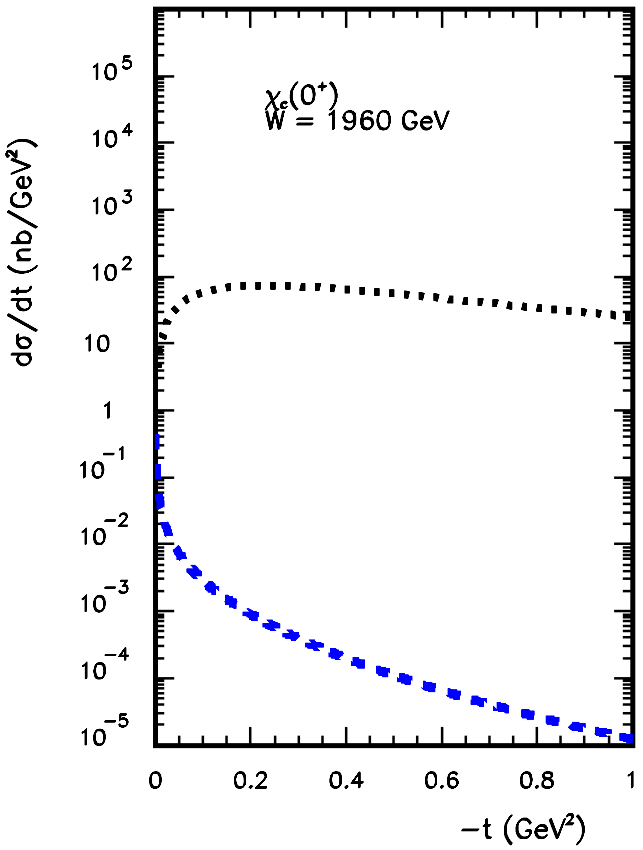

FIG. 27 (color online). Distribution in $t = t_1 = t_2$ for two-photon (dashed, blue line) and the phenomenological two-Pomeron (dotted line) fusion. Compare these distributions with those obtained in the QCD approach in Fig. 20.

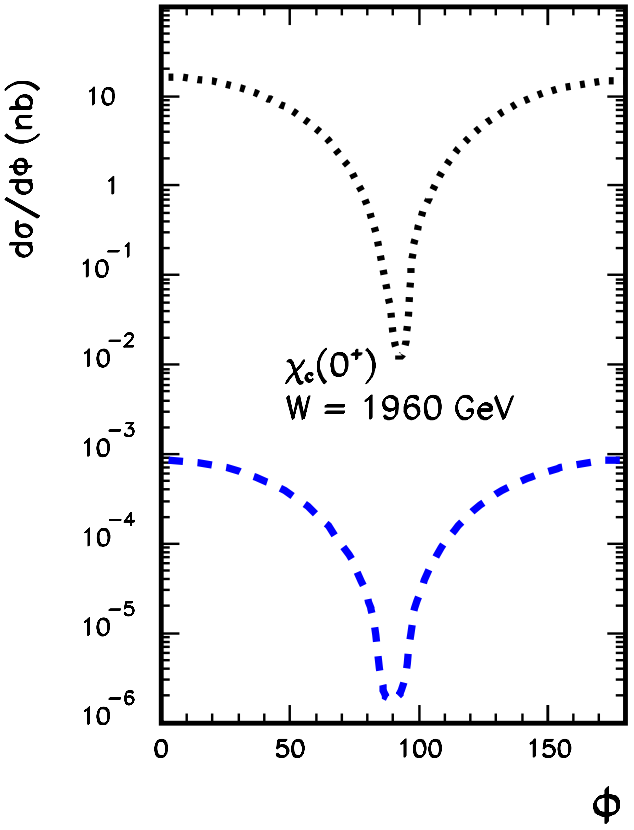

FIG. 28 (color online). Distribution in relative azimuthal angle Φ for two-photon (dashed, blue line) and two-Pomeron (dotted line) fusion. Compare these distributions with those obtained in the QCD approach in Fig. 21.

in the not too distant future. Only then a detailed comparison is justified.

C. Energy dependence

Up to now we have concentrated on Tevatron energy. We expect some results for the exclusive χ_c production in the not too distant future. It would be also interesting to measure exclusive χ_c production at different energies. The obvious choices are RHIC and LHC in the near future. In Fig. 29 we show distributions in x_F for different UGDFs for RHIC, $W = 200$ GeV (left panel) and LHC, $W = 14\,000$ GeV (right panel). When compared to Tevatron the distributions in x_F for RHIC are wider and the distributions for LHC are more narrow, concentrated around $x_F = 0$. At the RHIC energy the different UGDFs give relatively similar results, whereas at the LHC energy there is a difference of several orders of magnitude between results obtained with different UGDFs. Therefore a measurement at LHC should clearly select the best distribution.

In Table II we have collected total cross sections for some selected UGDFs at RHIC, Tevatron, and LHC. Comparing the results for the three different energies we see that different UGDFs predict completely different energy dependence. While BFKL predicts a strong growth of the cross section with the collision energy, the saturation models (KL, GBW) predict much slower rise with the collision energy. Therefore measuring the exclusive $\chi_c(0^+)$ produc-

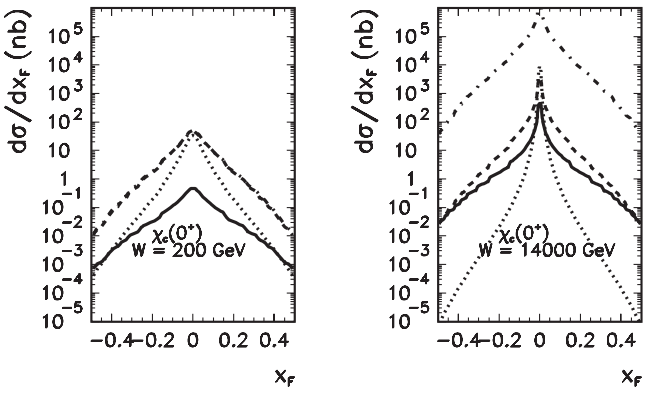

FIG. 29. Distribution in x_F of $\chi_c(0^+)$ meson for different UGDFs. The left (right) panel shows the results for RHIC (LHC). The meaning of lines is as for the Tevatron energy.

TABLE II. Integrated cross section $\sigma_{\rm tot}$ (in nb) for exclusive $\chi_c(0^+)$ production at different energies. The numbers for Gaussian UGDF refer to the prescription in Eq. (2.35).

UGDF	RHIC	Tevatron	LHC
KL	0.6430(+1)	0.5231(+2)	0.1090(+3)
GBW	0.2830(+1)	0.1590(+3)	0.1413(+3)
BFKL	0.6140(+1)	0.1125(+4)	0.6306(+5)
Gauss, $\sigma_0 = 1.0$ GeV, scales (2)	0.7126(−1)	0.1811(+1)	0.1428(+2)

tion at three different energies would be useful to pin down the underlying dynamics.

VI. DISCUSSION AND CONCLUSIONS

In the present paper we have discussed in detail the exclusive production of the $\chi_c(0^+)$ meson in proton-antiproton and proton-proton collisions. We have considered both the diffractive and purely electromagnetic mechanisms. Many differential distributions have been discussed for the first time in the literature.

The diffractive component was calculated in the KMR approach. The only natural hard scale of the considered process is the quarkonium mass, as initially suggested by KMR. The dependence of the integrated cross section on this scale as well as on the nonperturbative cutoff is rather strong. This means that most of the cross section comes from the nonperturbative region.

When compared to the original KMR calculation we have taken into account the off shellness of gluons in the corresponding diagram. The corresponding matrix element was calculated. We find that the inclusion of the gluon virtualities reduces the cross section by a factor of 2–5, depending on the kinematical region and on UGDFs.

We have discussed the uncertainties in the KMR approach, both those related to the treatment of the nonperturbative region as well as those related to the choice of the scale and effective transverse momentum in their skewed unintegrated distributions. This gives an uncertainty factor of 2–3.

We get similar integrated cross section as in Ref. [21] if we take the on shell approximation for the vertex, make the same choice of scales, use the same integrated gluon distributions, etc. Summarizing, we find rather large uncertainties in the approach.

Many other UGDFs from the literature were also used to calculate distributions in the Feynman variable, x_F, in the squares of the four-momentum transfers (t_1 and t_2) in the nucleon lines, and in the relative azimuthal angle between outgoing protons. Correlations in t_1 and t_2 have been analyzed as well. The results depend strongly on the choice of UGDF. This is related to a particular sensitivity of the cross section for the reaction under consideration to the nonperturbative region of very small gluon transverse momenta. Therefore, a measurement of the differential distributions would be very helpful to test the unintegrated distributions in this region. At RHIC one could measure the $\pi^+\pi^-$ and/or K^+K^- decay channels. The ALICE experiment could probably use a similar method. At the Tevatron $\gamma\gamma$ or $\gamma J/\psi$ channels seem preferable.

In the present paper, we have calculated only the bare distributions. Those are subject to absorption effects. The absorption effects are usually included by multiplying the bare distributions by a soft gap survival probability. The survival probability was estimate as $S^2(\text{Tevatron}) \approx 0.05$ and $S^2(\text{LHC}) \approx 0.025$ [21]. Therefore absorption leads to a large reduction of the bare cross section. In principle, the absorption effects may modify also the shapes of differential distributions such as the transverse momentum distribution of the produced meson, the distributions in t_1 and t_2, as well as the azimuthal-angle correlations [54,57]. This requires a further detailed analysis which clearly goes beyond the scope of the present paper.

For completeness we have calculated also the cross section in a more phenomenological approach with Regge-type Pomeron-Pomeron fusion. Cross sections of the same order of magnitude as for the QCD approach are obtained. However, the azimuthal-angle correlation functions for both approaches are very different.

We have also calculated differential distributions for the photon-photon fusion. This contribution turned out to be rather small (a fraction of nb). The differential distributions have quite different shapes compared to the diffractive component. When compared to the diffractive component, it is peaked at extremely small values of t_1 and/or t_2. The pattern of azimuthal-angle correlations is also very different: $\cos\Phi$ for the $\gamma\gamma$ fusion, but has a more complicated shape for the diffractive component due to the loop integration in the formula for the amplitude.

Recently, there is some interest to study exclusive production of the J/ψ meson at Tevatron. This is because of a possibility to study J/ψ photoproduction at large energies [54] and due to a potential search for the odderon exchange [58]. Because of its decay channel $\chi_c(0^+) \to \gamma J/\psi$ and difficulties in identifying soft photons, the $\chi_c(0^+)$ decays may contribute to the "exclusive" production of J/Ψ and make the measurement of J/Ψ photoproduction and/or the discovery of the odderon exchange rather difficult. Thus a comparison of theoretical cross sections for the three mentioned reactions would be very useful. Our estimates for

Tevatron energies, including soft survival probability, give 20–200 nb times $\mathrm{BR}(\chi_c(0^+) \to \gamma J/\psi) = 0.013$ which gives the corresponding cross section rather less than 1 nb compared to about 15 nb for the J/ψ photoproduction [54].

We have also made the calculation of $d\sigma/dx_F$ distributions and total cross sections for RHIC and LHC. Comparing these results and those for the Tevatron leads to the conclusion that only measurements for different energies may help to disentangle the underlying QCD dynamics. In principle, such measurements could even explore the onset of QCD saturation which is not so easy to be discovered in inclusive reactions.

ACKNOWLEDGMENTS

The useful discussions with B. I. Ermolaev, F. Jegerlehner, A. B. Kaidalov, V. A. Khoze, N. I. Kochelev, W. Schäfer, and D. V. Shirkov are gratefully acknowledged. This work was partially supported by the Polish Ministry of Scientific Research and Information Technology Grant No. 1 P03B 028 28, the Russian Foundation for Fundamental Research, Grants No. 06-02-16215, No. 07-02-91557, and No. 08-02-00896-a, the Bogoliubov-Infeld Programme 2007, and the Russian Federation Ministry of Education and Science Grant No. MIREA 2.2.2.2.6546.

[1] V. A. Khoze, A. D. Martin, and M. G. Ryskin, Phys. Lett. B **401**, 330 (1997); Eur. Phys. J. C **23**, 311 (2002); A. B. Kaidalov, V. A. Khoze, A. D. Martin, and M. G. Ryskin, Eur. Phys. J. C **31**, 387 (2003); **33**, 261 (2004); V. A. Khoze, A. D. Martin, M. G. Ryskin, and W. J. Stirling, Eur. Phys. J. C **35**, 211 (2004).
[2] S. Heinemeyer, V. A. Khoze, M. G. Ryskin, W. J. Stirling, M. Tasevsky, and G. Weiglein, Eur. Phys. J. C **53**, 231 (2008).
[3] G. A. Schuler, CERN Report No. CERN-TH-7170-94, 1994.
[4] E. Braaten, S. Fleming, and T. C. Yuan, Annu. Rev. Nucl. Part. Sci. **46**, 197 (1996).
[5] P. Nason *et al.*, arXiv:hep-ph/0003142.
[6] N. Brambilla *et al.* (Quarkonium Working Group), Reports No. FERMILAB-FN-0779 and CERN-2005-005, 2004, pp. 521.
[7] M. Kramer, Prog. Part. Nucl. Phys. **47**, 141 (2001).
[8] P. Hagler, R. Kirschner, A. Schafer, L. Szymanowski, and O. Teryaev, Phys. Rev. D **62**, 071502 (2000);Ph. Hagler, R. Kirschner, A. Schafer, L. Szymanowski, and O. V. Teryaev, Phys. Rev. D **63**, 077501 (2001).
[9] A. V. Lipatov, V. A. Saleev, and N. P. Zotov, arXiv:hep-ph/0112114; S. P. Baranov, A. V. Lipatov, and N. P. Zotov, Yad. Fiz. **67**, 856 (2004).
[10] S. Catani, M. Ciafaloni, and F. Hautmann, Phys. Lett. B **242**, 97 (1990); Nucl. Phys. **B366**, 135 (1991).
[11] J. C. Collins and R. K. Ellis, Nucl. Phys. **B360**, 3 (1991).
[12] G. Camici and M. Ciafaloni, Phys. Lett. B **386**, 341 (1996); Nucl. Phys. **B496**, 305 (1997).
[13] M. G. Ryskin, A. G. Shuvaev, and Yu. M. Shabelski, Phys. At. Nucl. **64**, 120 (2001).
[14] V. S. Fadin and L. N. Lipatov, Nucl. Phys. **B477**, 767 (1996); V. S. Fadin, R. Fiore, A. Flachi, and M. I. Kotsky, Phys. Lett. B **422**, 287 (1998); V. Fadin, in *BFKL News, LAFEX School on High Energy Physics (LISHEP98), February 14-21, Rio de Janeiro, Brazil, 1998*, (High Energy Physics, Rio de Janeiro, 1998), pp. 742-776.
[15] L. Lonnblad and M. Sjödahl, J. High Energy Phys. 05 (2005) 038; J. High Energy Phys. 02 (2004) 042.
[16] J. R. Forshaw, Proc. Sci., DIFF2006 (2006) 055 [arXiv: hep-ph/0611274].
[17] V. A. Petrov and R. A. Ryutin, J. High Energy Phys. 08 (2004) 013.
[18] T. Affolder *et al.* (CDF Collaboration), Phys. Rev. Lett. **88**, 151802 (2002); D. E. Acosta *et al.* (CDF Collaboration), Phys. Rev. Lett. **91**, 011802 (2003); K. Terashi (CDF Collaboration), arXiv:0705.3804; CDF Collaboration, CDF note 8493 (unpublished).
[19] O. Kepka and C. Royon, Phys. Rev. D **76**, 034012 (2007).
[20] F. Yuan, Phys. Lett. B **510**, 155 (2001).
[21] V. A. Khoze, A. D. Martin, M. G. Ryskin, and W. J. Stirling, Eur. Phys. J. C **35**, 211 (2004).
[22] A. K. Likhoded and A. V. Luchinsky, Phys. At. Nucl. **71**, 294 (2008).
[23] V. A. Saleev and D. V. Vasin, Phys. Lett. B **548**, 161 (2002); Phys. Rev. D **68**, 114013 (2003); B. A. Kniehl, D. V. Vasin, and V. A. Saleev, Phys. Rev. D **73**, 074022 (2006); B. A. Kniehl, V. A. Saleev, and D. V. Vasin, Phys. Rev. D **74**, 014024 (2006).
[24] P. Hagler, R. Kirschner, A. Schafer, L. Szymanowski, and O. V. Teryaev, Phys. Rev. Lett. **86**, 1446 (2001).
[25] B. Guberina, J. H. Kuhn, R. D. Peccei, and R. Rückl, Nucl. Phys. **B174**, 317 (1980).
[26] R. Baier and R. Ruckl, Z. Phys. C **19**, 251 (1983).
[27] P. L. Cho and A. K. Leibovich, Phys. Rev. D **53**, 150 (1996); **53**, 6203 (1996).
[28] J. H. Kuhn, Phys. Lett. **89B**, 385 (1980); J. H. Kuhn, J. Kaplan, and E. G. O. Safiani, Nucl. Phys. **B157**, 125 (1979).
[29] A. Szczurek, R. S. Pasechnik, and O. V. Teryaev, Phys. Rev. D **75**, 054021 (2007).
[30] J. R. Forshaw, arXiv:hep-ph/0508274.
[31] Yu. A. Simonov, Yad. Fiz. **58**, 113 (1995) [Phys. At. Nucl. **58**, 107 (1995); A. M. Badalian and Yu. A. Simonov, Yad. Fiz. **60**, 714 (1997) [Phys. At. Nucl. **60**, 714 (1997)].
[32] Yu. L. Dokshitzer, V. A. Khoze, and S. L. Troyan, Phys. Rev. D **53**, 89 (1996).
[33] G. Grunberg, Phys. Lett. B **372**, 121 (1996).
[34] D. V. Shirkov and I. L. Solovtsov, Phys. Rev. Lett. **79**, 1209 (1997).
[35] A. I. Alekseev and B. A. Arbuzov, Mod. Phys. Lett. A **13**,

1747 (1998).
[36] B. R. Webber, J. High Energy Phys. 10 (1998) 012.
[37] C. S. Fischer and R. Alkofer, Phys. Rev. D **67**, 094020 (2003).
[38] G. M. Prosperi, M. Raciti, and C. Simolo, Prog. Part. Nucl. Phys. **58**, 387 (2007).
[39] M. Glück, E. Reya, and A. Vogt, Z. Phys. C **67**, 433 (1995); Eur. Phys. J. C **5**, 461 (1998).
[40] M. B. Cakir and G. R. Farrar, Phys. Rev. D **50**, 3268 (1994).
[41] F. E. Close, G. R. Farrar, and Z. P. Li, Phys. Rev. D **55**, 5749 (1997).
[42] R. S. Pasechnik, O. V. Teryaev, and A. Szczurek, Eur. Phys. J. C **47**, 429 (2006).
[43] A. Donnachie and P. V. Landshoff, Phys. Lett. B **185**, 403 (1987); **191**, 309 (1987); Nucl. Phys. **B303**, 634 (1988).
[44] B. Pire, J. Soffer, and O. Teryaev, Eur. Phys. J. C **8**, 103 (1999).
[45] J. Bartels, S. Bondarenko, K. Kutak, and L. Motyka, Phys. Rev. D **73**, 093004 (2006).
[46] M. Łuszczak and A. Szczurek, Phys. Rev. D **73**, 054028 (2006).
[47] K. Golec-Biernat and M. Wüsthoff, Phys. Rev. D **60**, 114023 (1999).
[48] D. Kharzeev and E. Levin, Phys. Lett. B **523**, 79 (2001).
[49] E. A. Kuraev, L. N. Lipatov, and V. S. Fadin, Zh. Eksp. Teor. Fiz. **72**, 377 (1977) [Sov. Phys. JETP **45**, 199 (1977)]; Ya. Ya. Balitskij and L. N. Lipatov, Yad. Fiz. **28**, 1597 (1978) [Sov. J. Nucl. Phys. **28**, 822 (1978).].
[50] M. A. Kimber, A. D. Martin, and M. G. Ryskin, Eur. Phys. J. C **12**, 655 (2000); Phys. Rev. D **63**, 114027 (2001).
[51] M. Drees and D. Zeppenfeld, Phys. Rev. D **39**, 2536 (1989).
[52] W. M. Yao *et al.* (Particle Data Group), J. Phys. G **33**, 1 (2006).
[53] A. Donnachie and P. V. Landshoff, Phys. Lett. B **296**, 227 (1992).
[54] W. Schäfer and A. Szczurek, Phys. Rev. D **76**, 094014 (2007).
[55] M. Gallinaro (CDF Collaboration), Acta Phys. Pol. B **35**, 465 (2004).
[56] M. Rangel, C. Royon, G. Alves, J. Barreto, and R. Peschanski, Nucl. Phys. **B774**, 53 (2007).
[57] V. A. Khoze, A. D. Martin, and M. G. Ryskin, J. High Energy Phys. 05 (2006) 036.
[58] A. Bzdak, L. Motyka, L. Szymanowski, and J.-R. Cudell, Phys. Rev. D **75**, 094023 (2007).